Nonlinear Wave Loads on Offshore Structures

by

Jonny Klepsvik

Submitted to the Department of Ocean Engineering
in partial fulfillment of the requirements for the degree of

Master of Science in Ocean Engineering

at the

MASSACHUSETTS INSTITUTE OF TECHNOLOGY

May 1995

Author .....
.....
Department of Ocean Engineering
May 12, 1995

Certified by .....
J. Nicholas Newman
Professor of Naval Architecture
Thesis Supervisor

Accepted by ....
.....
A. Douglas Carmichael
Chairman, Departmental Committee on Graduate Students

Nonlinear Wave Loads on Offshore Structures

by

Jonny Klepsvik

Submitted to the Department of Ocean Engineering
on May 12, 1995, in partial fulfillment of the
requirements for the degree of
Master of Science in Ocean Engineering

Abstract

Wave Loads up to the third-order are predicted, based on the FNV-theory, for a cylinder and the Draugen monotower platform exposed to long regular waves. The first-order problem is solved using WAMIT to obtain the added mass and wave damping to be used in the prediction of the higher-order pitch motion. The principle of superposition is used to find the pitch response due to the higher-order wave loads.

The computed results are compared to model test results of Draugen and found to compare well. The higher-order wave effects are found to become increasingly important for higher wavenumbers Ka.

Thesis Supervisor: J. Nicholas Newman
Title: Professor of Naval Architecture

Acknowledgments

I would like to to thank my advisor, Professor J. N. Newman, for his many helpful advices and comments not only troughout this work, but throughout my whole time here at M.I.T.. I also want to thank all the members of the CHF group for their contributions and suggestions to the many problems that arose throughout this work.

Special thanks are due to Dr. Rick Mercier from Shell Houston, who provided the model test data from the DMI Draugen model test.

Contents

List of Figures

Chapter 1

Introduction

The analysis of wave effects on large offshore structures, such as wave loads and corresponding responses, are of great importance to ocean engineers in the design, and for the operational safety of offshore structures. The effects of ocean waves on large offshore structures are usually analyzed using potential theory, assuming viscous effects to be negligble.

The calculation of first order wave effects are now considered straightforward. More attention has been brought to the matter of calculating higher order wave effects. For tension leg platforms (TLPs) it has been observed that second order wave loads can cause resonant axial deflection of the tendons. This phenomenon is known as *springing.*

Recently, it has been noticed that in severe sea states, TLPs and 'monotowers' can experience a transient resonance condition at their natural frequencies substantially higher than the dominant wave frequency (Faltinsen *et al.*, 1995). This phenomenon cannot be explained by traditional first and second order theories. It appears to be a higher-order effect which has become known as *ringing. Ringing* occurs as axial deflection of the tendons of TLPs, and as structual deflection in the bending mode for 'monotowers'.

The cause of *ringing* is not yet completely understood. It has been observed that *ringing* tends to occur when the waves are steep and the wave amplitude is of the same order as the radius of the structure. However, there are some controversies

among researchers whether the non-linear wave kinematics or the non-linearity due to waves interacting with the structure is the most important factor. Researchers are going in many different directions in order to obtain the third order loads correctly and to explain the cause of *ringing*. One approach has been to extend the Morison equation, which gives good estimates for the first order wave loads in long waves, to predict higher order wave loads (Madsen, 1986), and (Rainey, 1989). Jefferys & Rainey (1994) have used this method to predict *ringing*.

Another approach has been presented by Malenica & Molin (1995). They obtain the complete third order velocity potential for a fixed cylinder in finite depth based on the traditional Stoke's perturbation method. The second order wave potential is an expansion of the first order potential, and is expressed in terms of this potential. The third order potential is obtained in a similar way. The wave loads calculated from the third order potential are compared with experimental results, but there is a large scatter between the results, so the comparison does not fully validate the numerical results.

Recently, Faltinsen *et al.* (1995) have presented another theory known as the FNV-theory, named after the authors initials (Faltinsen, Newman, and Vinje). The FNV-theory is based on the long wavelength approximation. In an inner domain close to the body surface the wave elevation is assumed to be significantly affected by non-linearities due to the presence of the structure causing wave diffraction and scattering. The first order wave potential is expanded up to the third order and a correction for the higher order scattering potential is added to the linear diffraction potential. The computed third order wave loads are found to overlap with the results from Malenica & Molin only for very small values of the non-dimensional wave number ka.

In order to establish a valid theory for third order wave loads, 'exact' results from model tests or full-scale tests are needed. Unfortunately, there is not a reliable method to distinguish third order loads from first, and second order loads when performing model tests. The need of comparing numerical results to experimental results has motivated the present study, where the third order wave loads and responses of a monotower platform are predicted, based on the FNV-theory. The higher order

wave effects are concentrated in a region close to the free surface, which lead to the expectation that higher order loads for a cylinder will be comparable to those of a monotower of slowly varying radius. The non-linearities due to interaction between incoming waves of different frequencies are assumed to be negligible. An unidirectional irregular incident wave field can than be obtained by superposition of regular waves. The wave loads and responses can be related to the incoming velocity field (Newman, 1994).

The first order problem is solved using WAMIT. Added mass and wave damping obtained from WAMIT is used in the calculation of the pitch response due to higher order wave loads. Model test results of the Draugen 'monotower' platform are compared to the numerical results.

Chapter 2

Theoretical Analysis

2.1 The Complete Boundary Value Problem

The diffraction potential of a body of arbritary shape, extending from the sea bottom, piercing the free surface, can be expressed as

$$\phi_D = \phi_I + \phi_S, \tag{2.1}$$

where ϕ_I is the incident wave potential and ϕ_S is the scattering potential, due to wave scattering, caused by the presence of the body. For a fixed body ϕ_D represents the total wave potential. However, if the body is allowed to move, a radiation potential due to the body motion is contributing to the velocity potential. The total velocity potential then becomes

$$\Phi = \phi_D + \phi_R, \tag{2.2}$$

where ϕ_R is the radiation potential. The complete boundary value problem can be described as

$$\nabla^2 \Phi = 0, \tag{2.3}$$

throughout the fluid domain.

$$\frac{\partial \Phi}{\partial n} = 0, \tag{2.4}$$

on the body surface. For finite water depths

$$\frac{\partial \Phi}{\partial z} = 0, \tag{2.5}$$

at $z = -h$. In the case of infinite water depth

$$\frac{\partial \Phi}{\partial z} \to 0, \tag{2.6}$$

as $h \to -\infty$. The free surface boundary condition is given as

$$\frac{\partial^2 \Phi}{\partial^2 t} + g\frac{\partial \Phi}{\partial y} = -2\nabla\Phi \cdot \nabla\frac{\partial \Phi}{\partial t} - \frac{1}{2}\nabla\Phi \cdot \nabla(\nabla\Phi \cdot \nabla\Phi). \tag{2.7}$$

To complete the boundary value problem the velocity potential must satisfy the radiation condition, which states that reflected waves must radiate outwards from the body to infinity.

Solving the complete boundary value problem is rather complicated due to the inhomogeneous free surface boundary condition. The traditional approach to handle this problem is to use Stokes' perturbation method, transferring the free surface boundary condition to the undisturbed plane of the free surface $z = 0$. However, recently Faltinsen *et al.*(1995) have presented another approach, where the free surface boundary condition is imposed on the moving plane $\eta_1 = A\sin\omega t$. This is further described in the next section.

2.2 The FNV-theory

Recently O.M. Faltinsen, J.N. Newman, and T. Vinje have presented a theory for predicting nonlinear wave loads on a fixed slender vertical cylinder. The regime where the wave amplitude A and cylinder radius a are of the same order, and both are small compared to the wavelength is considered. The diffraction problem is divided into an outer and an inner domain. Conventional linear analysis applies in the outer domain far from the cylinder. However, in the inner domain significant nonlinear effects exist associated with the free-surface boundary condition. The long wavelength approximation is justified in the inner domain when the wavelength λ is much larger than the cylinder radius a, $\lambda \gg a$. This is essentially the same as $Ka \ll 1$, where $K = \frac{2\pi}{\lambda}$ is the wavenumber. The wave amplitude A is of the same order as the cylinder radius a, $A/a = O(1)$. Thus the perturbation expansion of the inhomogeneous free-surface boundary condition is imposed on a horizontal plane which moves up and down with the incident wave at the center of the cylinder, $z = A\sin\omega t$, instead of at the plane $z = 0$ as in traditional perturbation expansions.

2.2.1 Unidirectional Regular Waves

Linear Analysis

For incoming regular waves of amplitude A and wave number K, the incident velocity potential for infinite water depth, in Cartesian coordinates (x, y, z), can be written as

$$\phi_I = Re\{(\frac{gA}{\omega})\exp(Kz - iKx + i\omega t)\}, \tag{2.8}$$

where ω is the wave frequency. Alternatively and more appropriate for the case of a circular cylinder, the velocity potential can be expressed in cylindrical coordinates (r, θ, z) as

$$\phi_I = Re\{(\frac{gA}{\omega}\exp(Kz + i\omega t)\sum_{m=0}^{\infty}\epsilon_m i^{-m}\cos m\theta J_m(Kr)\}, \tag{2.9}$$

where $\epsilon_0 = 1$, $\epsilon_m = 2$ for $m > 0$, and J_m is the Bessel function of order m.

The total diffraction potential is given to the first order as $\phi_D = \phi_I + \phi_S$, where ϕ_S is the scattered potential. For a fixed cylinder of radius a, and by imposing the boundary condition $\frac{\partial\phi}{\partial n} = 0$ on the body surface, the scattered potential valid for all values of ka has been given by MacCamy & Fuchs (1954) as

$$\phi_S = -Re\{\frac{gA}{\omega}\exp(Kz + i\omega t)\sum_{m=0}^{\infty}\epsilon_m i^{-m}\cos m\theta\frac{H_m^{(2)}(Kr)J_m'(Ka)}{H_m^{(2)'}(Ka)}\}, \tag{2.10}$$

where $H_m^{(2)} = J_m - iY_m$ is the Hankel function of the second kind. For large Kr this potential has a periodic form that propagates away from the body, satisfying the radiation condition. In the inner domain, the expansion of the Hankel function of argument Kr can be used to find an approximation for ϕ_S. The main contribution of this expansion comes from the term $m = 1$ and is of order ϵ^2,

$$\phi_S \simeq -Re\{\frac{igA}{\omega}\exp(Kz + i\omega t)\cos m\theta\frac{Ka^2}{r}\}. \tag{2.11}$$

Adding ϕ_I and ϕ_S gives the total linear diffraction potential valid for the inner region as

$$\phi_D = Re\{\frac{gA}{\omega}\exp(Kz + i\omega t)[1 - iK\cos\theta(r + \frac{a^2}{r})]\} + O(\epsilon^3). \tag{2.12}$$

Faltinsen *et al.* present a higher order extension of (2.12) obtained from (2.10) as

$$\phi_D = Re\{\frac{gA}{\omega}\exp(Kz + i\omega t)[1 - iK(r + \frac{a^2}{r})\cos\theta - \frac{1}{4}K^2r^2$$

$$+\frac{1}{2}K^2a^2(\log\frac{1}{2}Kr+\gamma+\frac{\pi i}{2})-\frac{1}{4}K^2\cos 2\theta(r^2+\frac{a^4}{r^2})]\}+O(\epsilon^4). \tag{2.13}$$

The Higher Order Correction to ϕ_D

The higher order expansion leading to the potential given in (2.13) is inconsistent in the sense that terms of order Aa^2 are included, but nonlinear terms of order A^2a and A^3 are neglected. In the case when the wave amplitude A is of the same order as the cylinder radius a, $A/a = O(1)$, these terms will all be of comparable magnitude.

The corrected potential is expressed as

$$\Phi = \phi_D + \psi + O(\epsilon^4), \tag{2.14}$$

where ψ is the nonlinear correction potential. The principal boundary conditions for ψ are

$$\psi_r = 0 \tag{2.15}$$

on $r = a$, and

$$\psi_{tt} + g\psi_z = -2\nabla\Phi\cdot\nabla\Phi_t - \frac{1}{2}\nabla\Phi\cdot\nabla(\nabla\Phi)^2, \tag{2.16}$$

on $z = \eta$. The free-surface elevation η is defined as

$$\eta = -\frac{1}{g}[\Phi_t + \frac{1}{2}(\nabla\Phi)^2]_{z=\eta}, \tag{2.17}$$

where η can be expanded in the form $\eta = \eta_1 + \eta_2 + \cdots$. The two first terms in this expansion are written as

$$\eta_1 = A \sin \omega t, \tag{2.18}$$

and

$$\eta_2 = -KA(r+\frac{a^2}{r}) \cos\theta \cos\omega t - \frac{1}{2}KA^2 \cos 2\omega t + KA^2(\frac{a^2}{r^2} \cos 2\theta + \frac{1}{2}\frac{a^4}{r^4}) \sin^2 \omega t. \tag{2.19}$$

A full derivation of the nonlinear correction potential can be found in Faltinsen *et al.*

Wave Loads

Following Faltinsen *et al.* the expression for the force acting on the cylinder in the x-direction is given as

$$F_x = \rho a \int_0^{2\pi} \cos\theta d\theta \int_{-h}^{0} (\Phi_t + \frac{1}{2}V^2)_{r=a} dz + \rho a \int_0^{2\pi} \cos\theta d\theta \int_0^{\eta} (\Phi_t + \frac{1}{2}V^2 + gz)_{r=a} dz. \tag{2.20}$$

The first-order force component derived from (2.12) is expressed as

$$F_1(z) = \rho a \int_0^{2\pi} \phi_{Dt} \cos\theta d\theta = 2\pi\rho g K A a^2 e^{Kz} \cos\omega t. \tag{2.21}$$

The second-order force component from (2.12) is given as

$$F_2(z) = \frac{1}{2}\rho g \int_0^{2\pi} (\nabla\phi_D)^2 \cos\theta d\theta = \frac{1}{2}\pi\rho g K^2 a^2 A^2 e^{2Kz} \sin 2\omega t. \tag{2.22}$$

$F_1(z)$ and $F_2(z)$ are the contributions between $z = -h$ and $z = 0$. The force coming

from the integration between $z = 0$ and $z = \eta_1$ is given as

$$F_{P1} = \rho a \int_0^{2\pi} \cos\theta d\theta \int_0^{\eta_1} (\phi_{Dt} + \frac{1}{2}\nabla\phi_D \cdot \phi_D)_{r=a} dz$$

$$= \pi\rho g K a^2 A^2 \sin 2\omega t + \frac{1}{2}\pi\rho g K^2 a^2 A^3 (\cos\omega t - \cos 3\omega t) + O(\epsilon^6). \tag{2.23}$$

The contribution between $z = \eta_1$ and $z = \eta$ is given as

$$F_{P2} = \rho a \int_0^{2\pi} \cos\theta d\theta \int_{\eta_1}^{\eta} p dz = -\pi\rho g k^2 a^2 A^3 \cos\omega t \cos 2\omega t$$

$$= -\frac{1}{2}\pi\rho g K^2 a^2 A^3 (\cos\omega t + \cos 3\omega t) + O(\epsilon^6), \tag{2.24}$$

where $p = -\rho g(z - \eta) + O(\epsilon^3)$. F_{P1} and F_{P2} can be considered to be "point" forces acting at the location of the incident wave elevation, η_1. The "point" force due to the correction potential ψ is given as

$$F_{P3} = \pi\rho g K^2 a^2 A^3 (\cos\omega t - \cos 3\omega t) + O(\epsilon^6). \tag{2.25}$$

The total force acting on the cylinder in the x-direction is the sum of the integrated forces F_1 and F_2 and the "point" forces F_{P1}, F_{P2}, and F_{P3}.

Collecting the force components of the same harmonic give the following expressions;

$$F_{H1} = [2\pi\rho g A a^2 (1 - e^{-Kh}) + \pi\rho g K^2 a^2 A^3] \cos\omega t, \tag{2.26}$$

$$F_{H2} = [\frac{1}{4}\pi\rho g K a^2 A^2(1 - e^{Kh}) + \pi\rho g K a^2 A^2] \sin 2\omega t, \tag{2.27}$$

and,

$$F_{H3} = -2\pi\rho g K^2 a^2 A^3 \cos 3\omega t. \tag{2.28}$$

The expression of the total moment will include a fourth harmonic. The moment about $z = -h$ gives the following expressions;

$$M_{H1} = [2\pi\rho g a^2 A(h - \frac{1}{K} + e^{-Kh}) + \frac{1}{2}\pi\rho g K a^2 A^3 + h\pi\rho g K^2 a^2 A^3] \cos \omega t, \tag{2.29}$$

$$M_{H2} = [\frac{1}{2}\pi\rho g K a^2 A(h - \frac{1}{2K} + \frac{1}{2K}e^{-2Kh}) + h\pi\rho g K a^2 A^2 + \frac{3}{2}\pi\rho g K^2 a^2 A^4] \sin 2\omega t, \tag{2.30}$$

$$M_{H3} = -[\frac{1}{2}\pi\rho g K a^2 A^3 + 2h\pi\rho g K^2 a^2 A^3] \cos 3\omega t, \tag{2.31}$$

and the contribution to the fourth harmonic from equation (2.28),

$$M_{H4} = -\pi\rho g K^2 a^2 A^4 \sin 4\omega t. \tag{2.32}$$

The complete expression for the fourth harmonic will also include contribution from higher-order effects than considered in this study.

2.2.2 Unidirectional Irregular Waves

Recently, Newman (1994) has extended the FNV-theory to a more practical case of unidirectional irregular waves. An irregular wavefield is created by the superposition of regular waves. The forces are related to the incident wave field, and the incident velocity potential at the cylinder axis is defined as

$$\phi_{I,x=0}(z,t) = \frac{gA}{\omega}\exp(Kz + i\omega t). \tag{2.33}$$

The velocity comonents u, w of this incident wave field on $x = 0$ can be expressed as

$$u(z,t) = Re\{-K^2\phi_{I,x=0}\} = Re\{-i\omega A\exp(Kz + i\omega t)\}, \tag{2.34}$$

and

$$w(z,t) = Re\{K\phi_{I,x=0}\} = Re\{\omega A\exp(Kz + i\omega t)\}. \tag{2.35}$$

The horizontal and vertical velocity gradients can be expressed as

$$u_x(z,t) = Re\{-iK^2\phi_{I,x=0}\} = Re\{-\frac{\omega^3 A}{g}\exp(Kz - i\omega t)\}, \tag{2.36}$$

and

$$w_x(z,t) = Re\{-K^2\phi_{I,x=0}\} = Re\{\frac{-i\omega^3 A}{g}\exp(Kz + i\omega t)\}. \tag{2.37}$$

The linear diffraction potential (2.13) can now be expressed in terms of $\phi_{I,x=0}$, u, and u_x as

$$\phi_D = Re\{\phi_{I,x=0}(1+C)\}+u(r+\frac{a^2}{r})\cos\theta+\frac{1}{4}u_x[r^2+\cos 2\theta(r^2+\frac{a^4}{r^2})-2a^2\log(\frac{r}{a})]+O(\epsilon)^3, \tag{2.38}$$

where $C = \frac{1}{2}(Ka)^2(\log\frac{1}{2}Ka + \gamma + \frac{\pi i}{2})$ is a complex constant of order $\epsilon^2\log\epsilon$.

The potential (2.38) applies in an irregular incident wave field defined on the cylinder axis by the time-varying functions $\phi_{I,x=0}$, u, and u_x, with the exception of the contribution from the constant C. However, in these analyses the higher-order constant C does not contribute.

The free-surface elevation is expressed as $\eta = \eta_1 + \eta_2\cdots$, where

$$\eta_1 = -\frac{1}{g}\phi_{It}, \tag{2.39}$$

and

$$\eta_2 = -\frac{1}{g}[\frac{1}{2}(u^2+w^2) - \eta_1] + \frac{u^2}{g}(\frac{a^2}{r^2}\cos 2\theta - \frac{1}{2}\frac{a^4}{r^4}) - \frac{u_t}{g}(r-\frac{a^2}{r})\cos\theta. \tag{2.40}$$

Wave Loads

From equation (2.20) the force contribution between $z = -h$ and $z = 0$ now becomes

$$F_1 = 2\pi\rho a^2 u_t \qquad\qquad O(KA), \tag{2.41}$$

and

$$F_2 = \pi\rho a^2(2ww_x + uu_x) \qquad\qquad O(KA)^2. \tag{2.42}$$

Neglecting difference frequencies, the right hand side of (2.42) can be replaced by either $\pi\rho a^2 w w_x$ or $-\pi\rho a^2 u u_x$. The force contribution between $z = 0$ and $z = \eta_1$ is given as

$$F_{P1} = \pi\rho a^2(2u_t\eta_1 + u_{tz}\eta_1^2 + 2wu_z\eta_1 - uw_z\eta_1). \tag{2.43}$$

The first term in (2.43) is of order $(KA)^2$ while the three last terms are of order $(KA)^3$. The contribution between $z = \eta_1$ and $z = \eta$, after neglecting difference-frequency components, becomes

$$F_{P2} = \pi\rho a^2\eta_1(u_{tz}\eta_1 + wu_z - \frac{2}{g}u_t w_t) \qquad O(KA)^3. \tag{2.44}$$

The "point" force contribution from the nonlinear potential ψ can be written as

$$F_{P3} = \frac{4\pi\rho a^2}{g}u^2 u_t \qquad O(KA)^3. \tag{2.45}$$

Organizing the force components according to the different powers of KA, the first, second, and third order force component can be expressed as;

$$F^{1st}(t) = 2\pi\rho a^2 u_t, \tag{2.46}$$

$$F^{2nd}(t) = \pi\rho a^2[-uu_x + 2u_t\eta_1], \tag{2.47}$$

and

$$F^{3rd}(t) = \pi\rho a^2[2wu_z\eta_1 - uw_z\eta_1 + 2u_{tz}\eta_1^2 - \frac{2}{g}u_t w_t\eta_1 + \frac{4}{g}u^2 u_t]. \tag{2.48}$$

Chapter 3

Problem Statement

3.1 Description of the Problem

The FNV-theory is applicable for a fixed circular cylinder of constant radius in infinite water depth. However, it can be extended to finite water depth by using the *ad hoc.* assumption that, if the cylinder is deep enough, the pressure distribution on the cylinder will not change much due to the presence of the sea bottom. In a water depth of 252.5 m, the waves are assumed to be deep water waves. Mathematically this is expressed as

$$\frac{\cosh[K(h+z)]}{\cosh Kh} \simeq e^{Kz}. \tag{3.1}$$

For deep water waves the dispersion relation simplifies from

$$\omega^2 = Kg \tanh \ Kh \tag{3.2}$$

to

$$\omega^2 = Kg. \tag{3.3}$$

A gravity based monotower platform with slowly varying radius can be approximated

as a circular cylinder. This approximation is obviously not good for calculation of the first order wave load, since the first order pressure field penetrates to large depths. However, higher order wave loads are concentrated in the free surface region, where the radius of the platform does not change much and can be assumed constant. The Draugen montower platform, which is considered in this study, has a part of constant radius in this region that makes the approximation even better. Based on the above approximations, the FNV-theory will be applied to estimate higher order wave loads acting on Draugen. The higher order excitation forces can be used in the linear equations of motions to predict the responses of the platform.

The first-order problem can be solved either in the frequency domain or the time domain. WAMIT operates in the frequency domain so a comparison between WAMIT and FNV results for a cylinder is made in this domain. The excitation force equals the diffraction force for a moving body in the first-order problem since

$$\frac{\partial \phi_S}{\partial n} = -\frac{\partial \phi_I}{\partial n} \tag{3.4}$$

is correct up to the first-order. However, (3.4) is not exact for the higher-order problem due to higher-order effects in the scattering potential. For small body motions, as in the case of this study, the equality (3.4) can be assumed to hold. The higher-order problem must be solved in the time domain.

For monotowers *ringing* is seen as a transient structural resonance phenomenon in the bending mode. Draugen has a natural period in pitch of 4.75 sec., since this is substantially higher than the dominant wave frequency, only the first bending mode is of significant interest associated with *ringing*. In the model test Draugen was modeled as free to move in pitch (rigid body motion), with an external spring at the moment point. If the external spring constant K_{EX} is very large, the structure can be approximated as clamped at the bottom. Then the motion will represent the first bending mode of the structure. The fact that the moment point was located at 55.9 m above the bottom makes this approximation even better. Only pitch motion is

considered in this study.

3.2 The Draugen DMI Model Test

The Draugen Danish Maritime Institute (DMI) model test data were provided by Shell in Houston. Figure 4.1 shows the platform configuration and Figure 3.1 shows the DMI model basin arrangement. The tests were performed at 1:50 scale and all data channels were sampled at 50 Hz (model scale) or 7.071 Hz (prototype scale). The model was segmented at the base of the shaft in order to simulate the first-mode response with a correct natural period. The "joint", which was placed at the bottom of the shaft, was arranged with low-friction linkage elements to allow the placement of load cells to measure shear force and overturning moment.

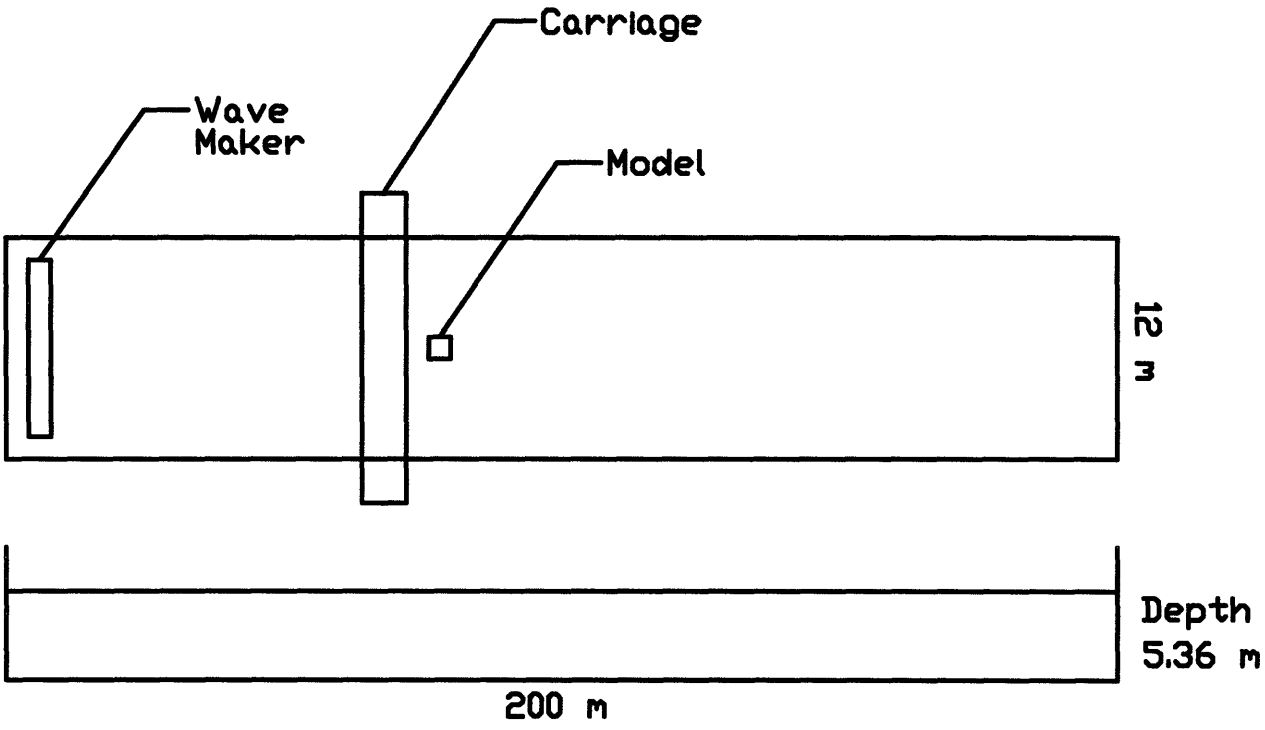

Figure 3-1: DMI Model Basin Arrangement

Nine channels of data were collected and below is a description of each collected data.

Channel	Description
1	wave elevation in meters at 50 m (prototype) to the side of the model
2	wave elevation in meters at leading edge of flare to the side of the model
3	wave elevation in meters at 50 m upwave of the model
4	transverse shear force (F_Y) in MN at the port side linkage
5	transverse shear force (F_Y) in MN at starboard side linkage
6	overturning moment (M_Y) in GMm at the joint
7	in-line deck displacement (D_X) in m
8	in-line deck acceleration (A_X) in $\frac{m}{s^2}$
9	in-line force (F_X) in GN at the joint

The transverse stiffness at the deck level was given to be 309 $\frac{MN}{m}$, which corresponds to a rotational stiffness at the moment point of $K_t = 1.57966e^{13}\frac{Nm}{\theta}$. K_t includes the hydrostatic coefficient and can be expressed as

$$K_t = K_{EX} + C_{55}. \tag{3.5}$$

The total mass of the platform was given as $m = 175,100$ tonnes.

Chapter 4

The First-Order Solution

4.1 First Order Solution from WAMIT

The first order problem is solved in the frequency domain for a circular cylinder of constant radius and for the Draugen 'monotower' platform. A geometric description of the body is needed in order to run WAMIT. The representation of the cylinder is straight forward, the mesh generation of Draugen, on the other hand, is more complicated. The platform configuration is shown in Figure 4.1.

4.1.1 Geometric Description of the Bodies

The platform is surrounded by seven stability cells at the bottom and the main shaft starts out with constant radius from the sea bottom up to El. = 76.7 m, where El. is the elevation measured from a reference plane at the bottom of the platform. The radius than starts changing linearly up to El. = 240.3 m, where the shaft has a section of constant radius before a flare section completes the structure. The water line Z=0 is at El. 252.5 m. The practical function of the flare section is to make a smooth transition from the circular cross-section of the shaft to the square cross-section of the platform deck. The flare starts under the mean free-surface in order to reduce slamming effects.

The cells at the bottom were modeled as a block of diameter d=79.5 m. The

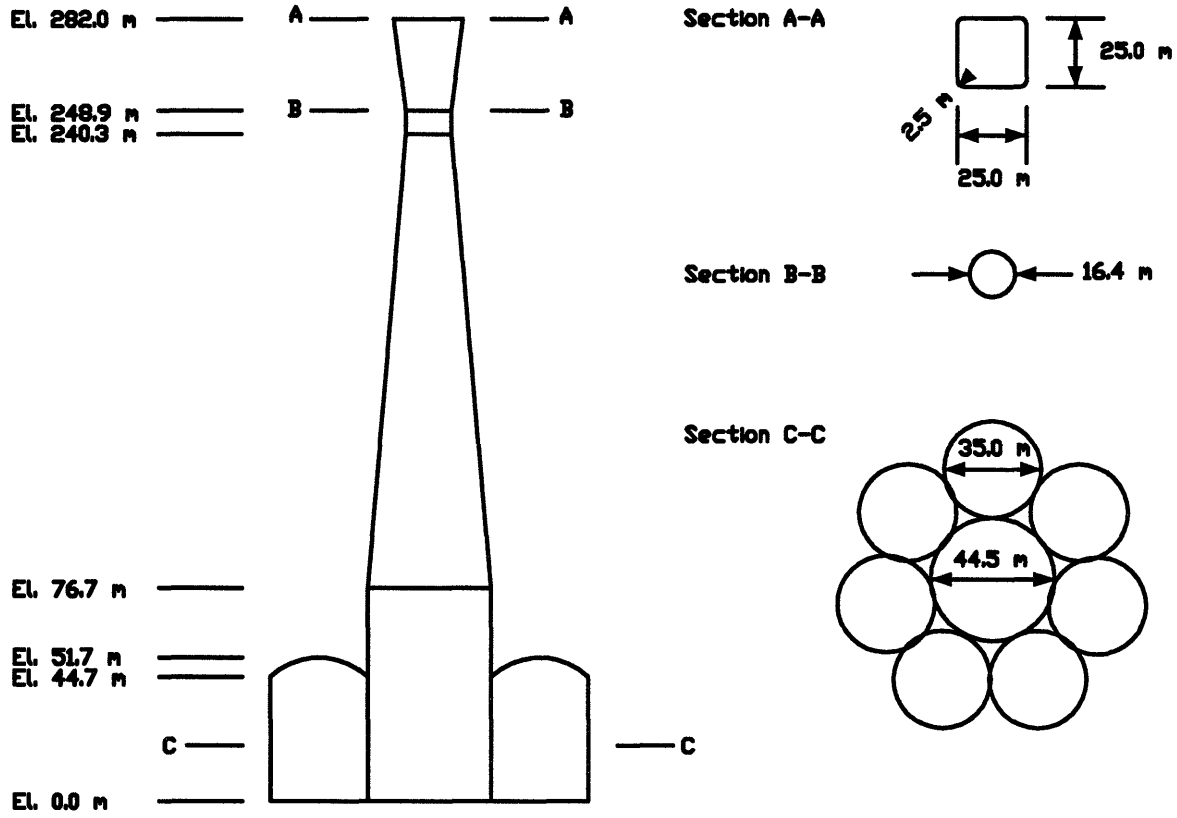

Figure 4-1: Platform Configuration of Draugen.

platform is fairly deep, and the structure is not moving much in response to the wave loads acting on it, so this is a good approximation. The surface piercing flare section, on the other hand, must be modeled with more care since the velocity potential in the free surface region is more sensible to the geometry of the body.

Figures 4.2 and 4.3 show the geometric description of the cylinder and Draugen, recpectively. Three different meshes with different numbers of panels were made for each geometry, this to ensure convergence. The coursest and finest meshes used are shown in Figures 4.2 and 4.3. In order to compare WAMIT results with results from the DMI model test, the moment point, which in WAMIT is taken as the origin of the body coordinates (x, y, z), was placed at $Z = -196.6$, where (X, Y, Z) are the global coordinates with $Z = 0$ at the mean free-surface. The geometric model of the platform was lifted 0.1 m above the sea bottom and the bottom of the platform was paneled. This was done to obtain the correct hydrostatic coefficient, C_{55} from WAMIT. The gap between the bottom and the platform will cause minimal numer-

ical problems in this case since the hydrodynamic disturbances at the bottom are very small. However, introducing a gap like this is not recommended and should be avoided if possible. The hydrostatic coefficient, C_{55} is expressed as

$$C_{55} = \rho g \int\int_{S_b} x^2 n_3 dS + \rho g \forall z_b - m g z_g, \tag{4.1}$$

where $\forall$ is the volume of the structure, z_g the vertical position of the center of gravity, and z_b the vertical position of the center of bouancy defined as

$$z_b = -\frac{1}{2\forall} \int\int_{S_b} z^2 dS. \tag{4.2}$$

The volume used to calculate z_b is given as

$$\forall = -\int\int_{S_b} n_3 z dS. \tag{4.3}$$

If no panels are defined on the bottom of the structure, the bottom surface will not be included in the surface integral in Equation (4.3), and the calculated volume will be wrong. The erroneous volume will cause z_b and C_{55} to be wrong as well. The center of gravity of Draugen was not known and not reported in the model test at DMI. I estimated the vertical position of the gravity to be at z_g=15.1 m, this based on the description of the platform. The 'exact' value of z_g is not important since the external stifness of the structure, K_t is dominating C_{55}.

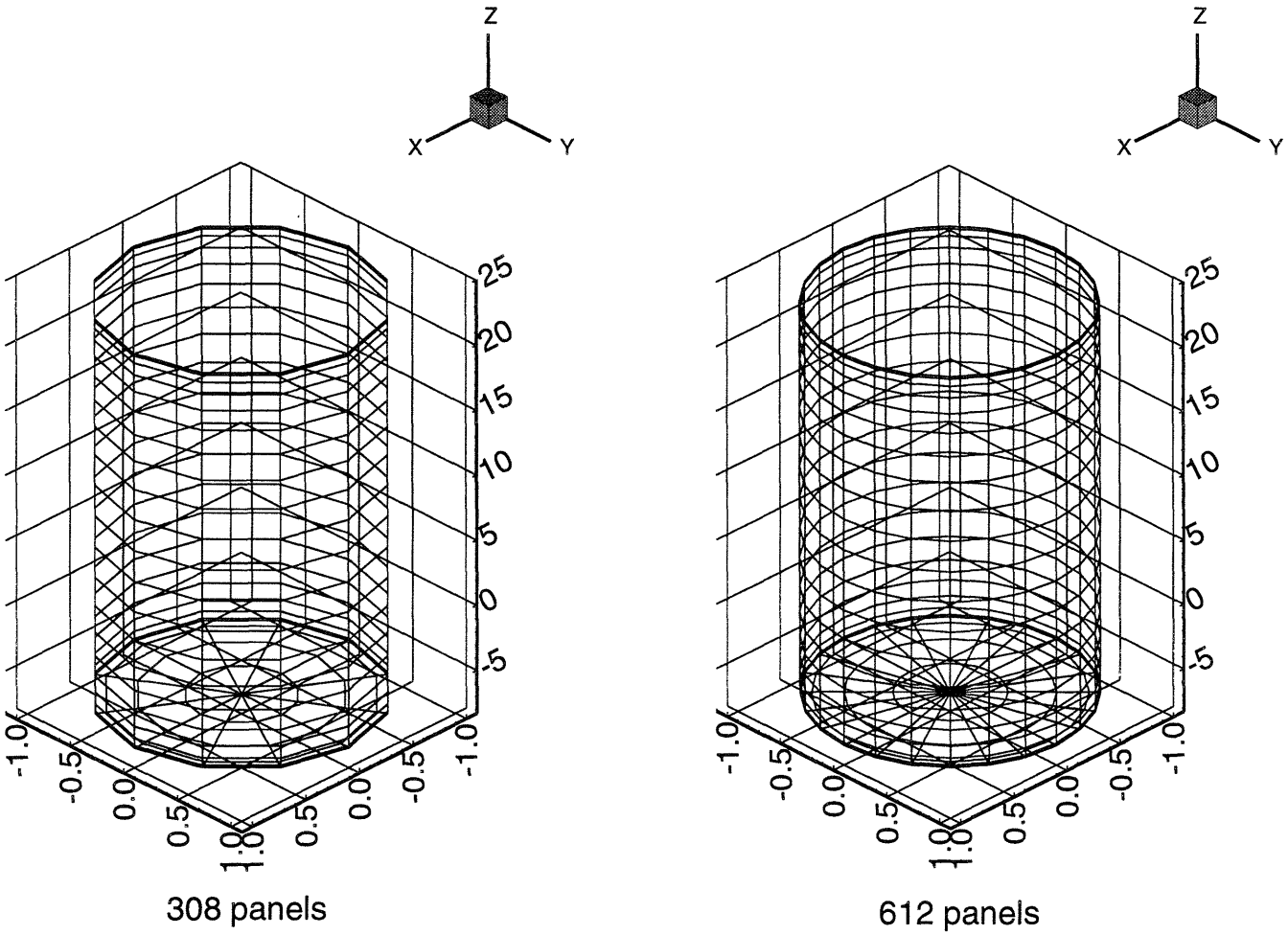

Figure 4-2: Discretization of the Cylinder

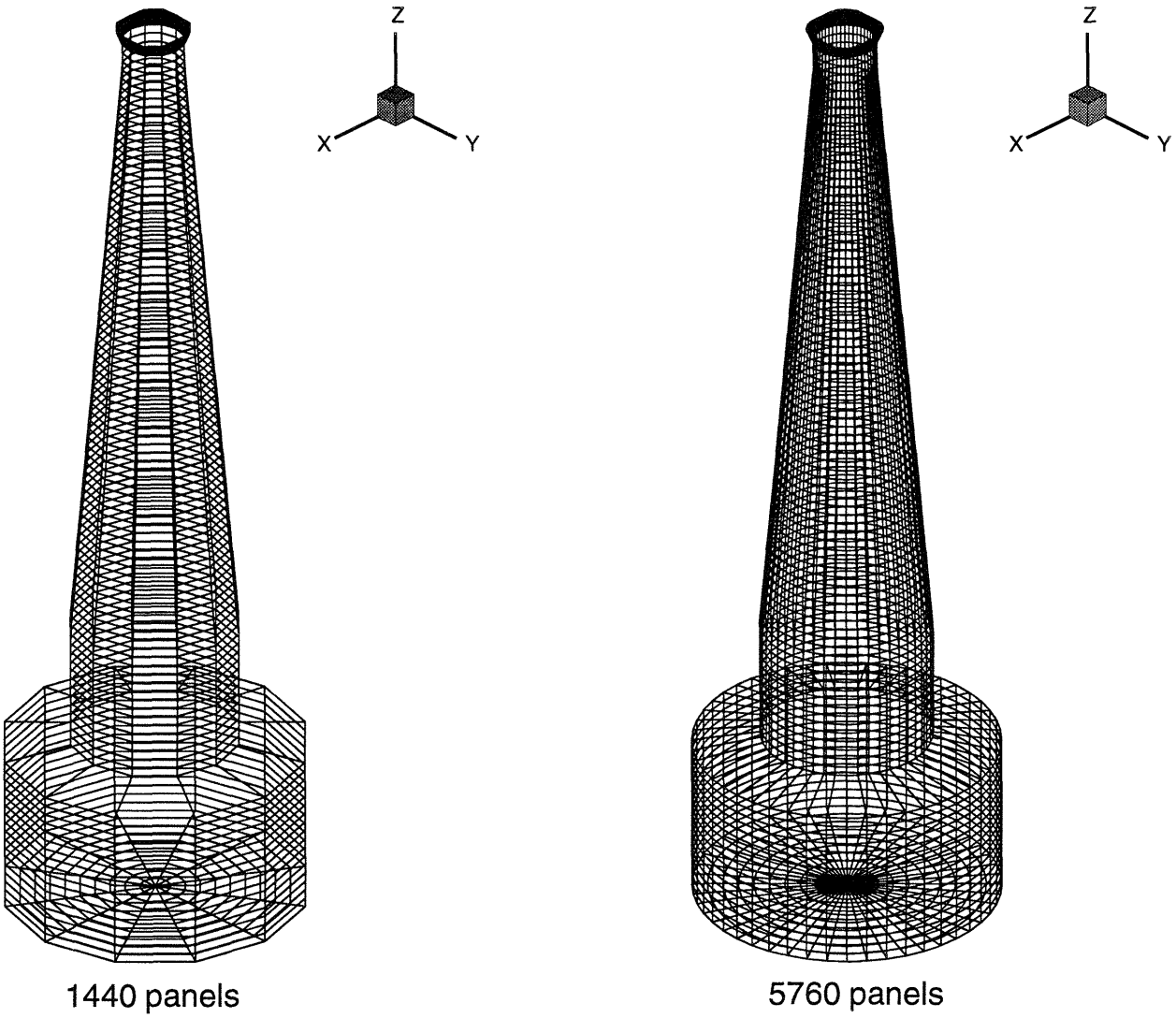

Figure 4-3: Panel Discretization of the Draugen Monotower Platform

4.1.2 First Order Wave Loads

The surge force and pitch moment are calculated for a cylinder of radius 8.2 m and for Draugen. The excitation force and moment obtained from direct integration of the hydrodynamic pressure is given as

$$X_i = -i\omega\rho \int\int_{S_b} n_i \phi_D dS. \tag{4.4}$$

Figures 4.4-3.4 show the surge force and pitch moment for the cylinder and Draugen obtained from WAMIT. The exitation forces are normalized as

$$\bar{X}_i = \frac{X_i}{\rho g A L^m}, \tag{4.5}$$

where m=2 for i=1,2,3 and m=3 for i=4,5,6.

In long waves the first order wave loads acting on Draugen are larger than those acting on the cylinder. Figures 4.4 and 4.6 show that the maximum surge force on Draugen is about six times that of the cylinder. However, the difference in pitch moment is not that significant. The rather large difference in the surge force is due to larger force contributions from the deeper part of Draugen compared to the cylinder. The force acting on the bodies below the moment point will create a stabilizing moment. This stabilizing moment is larger for Draugen than the cylinder which explains why the pitch moments are more comparable than the surge forces. Another way to put this is to argue that if the forces were concentrated in the free-surface region, the moment arm would have been large and the pitch moment would have been correspondingly large.

4.1.3 Added Mass, Damping, and Pitch Response

The added moment of inertia A_{55} and wave damping B_{55}, can be found by solving the radiation problem alone. The relation between A_{ij} and B_{ij} is given as

$$A_{ij} - \frac{i}{\omega} B_{ij} = \rho \int \int_{S_b} n_i \phi_j dS. \tag{4.6}$$

A_{55} and B_{55} are nondimensionalized as

$$\overline{A}_{55} = \frac{A_{55}}{\rho L^5}, \tag{4.7}$$

and

$$\overline{B}_{55} = \frac{B_{55}}{\rho L^5 \omega}. \tag{4.8}$$

Figures 4.8-4.10 show the added moment of inertia, wave damping, and the pitch response for Draugen, respectively. The pitch response is found by solving the diffraction and radiation problem. WAMIT allows one to define external mass, external damping, and external stifness. In order to compare results with the DMI test, external mass, and stiffness were defined in agreement with values used in the DMI model test. Only the natural frequency, and the stiffnes in the spring were known from the provided method. The external mass moment of inertia, I_{EX}, can be found from the relation

$$I_{EX} + A_{55} = K_t. \tag{4.9}$$

However, the added moment of inertia, A_{55}, had to be obtained from the radiation problem in order to find the external mass moment of inertia of Draugen.

It can be seen from Figure 4.8 that the added moment of inertia for Draugen

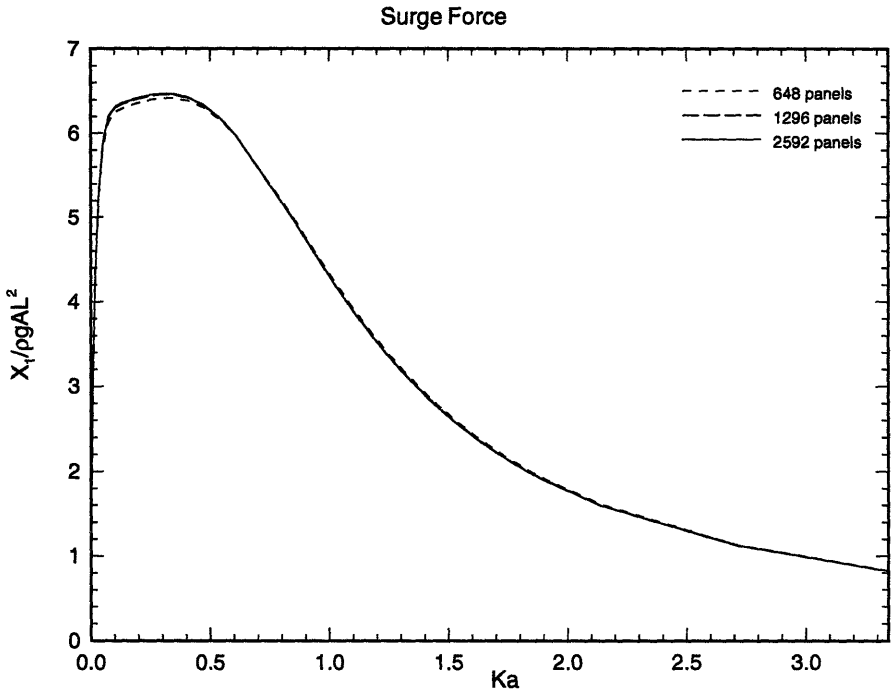

Figure 4-4: First Order Surge Force Acting on the Cylinder

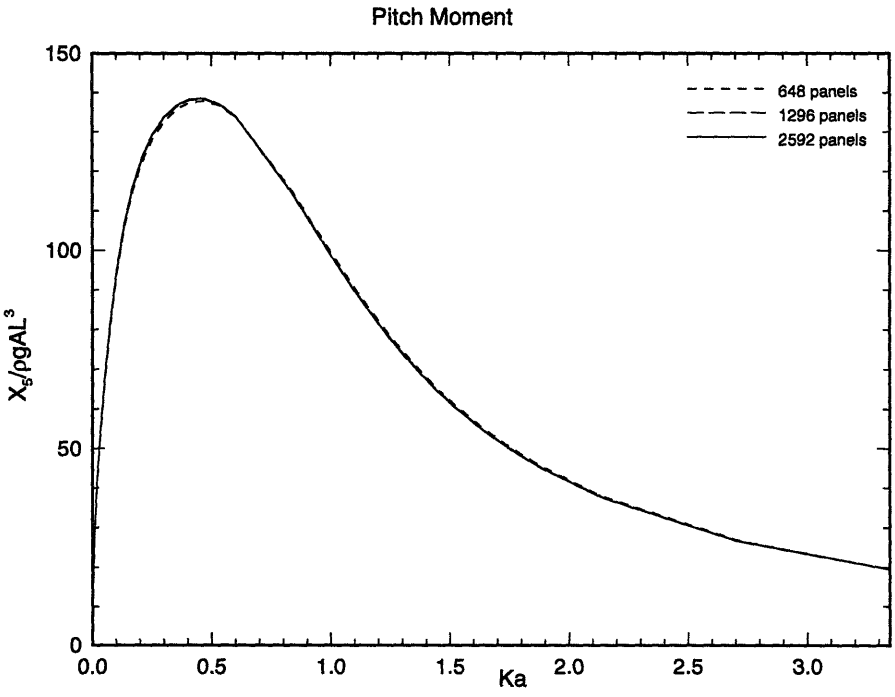

Figure 4-5: First Order Pitch Moment Acting on the Cylinder

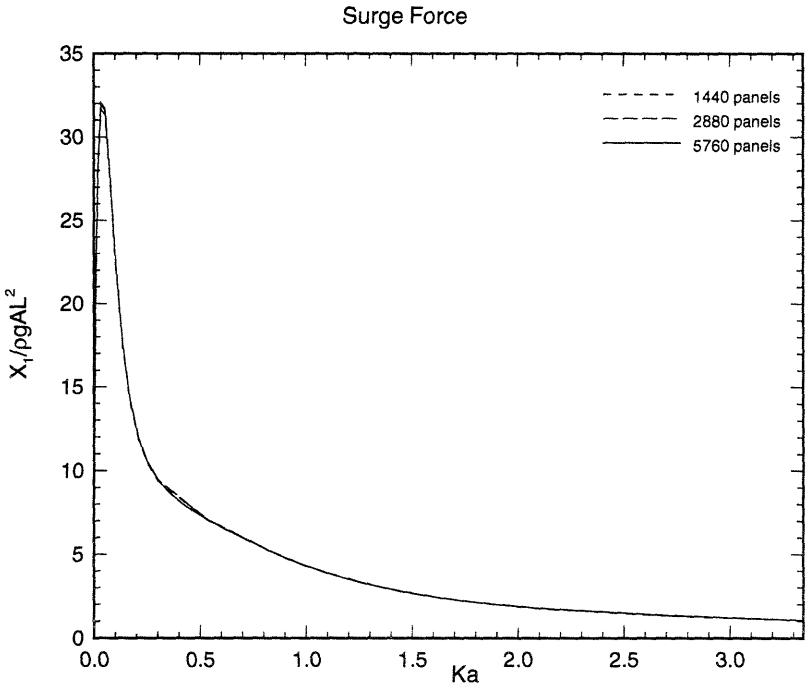

Figure 4-6: First Order Surge Force Acting on the Draugen

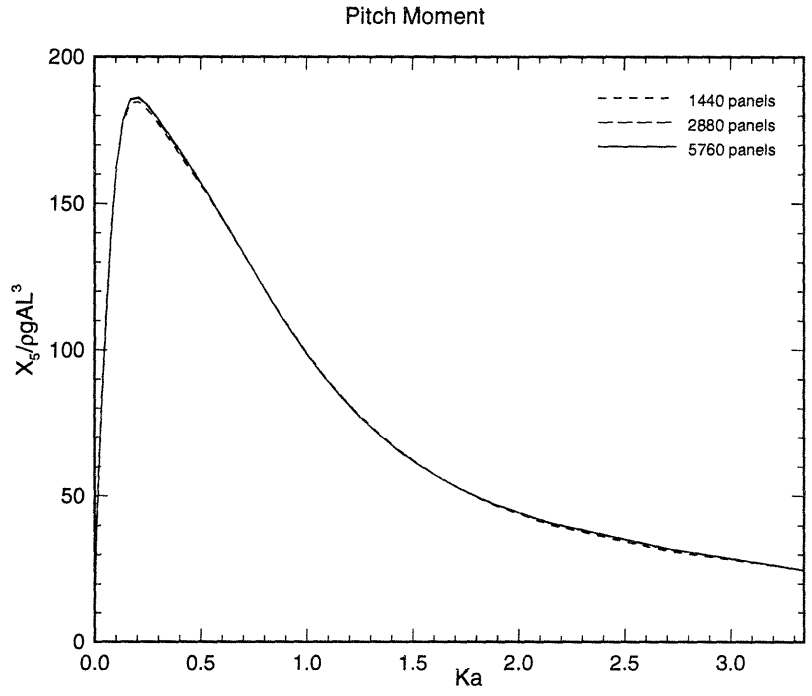

Figure 4-7: First Order Pitch Moment Acting on Draugen

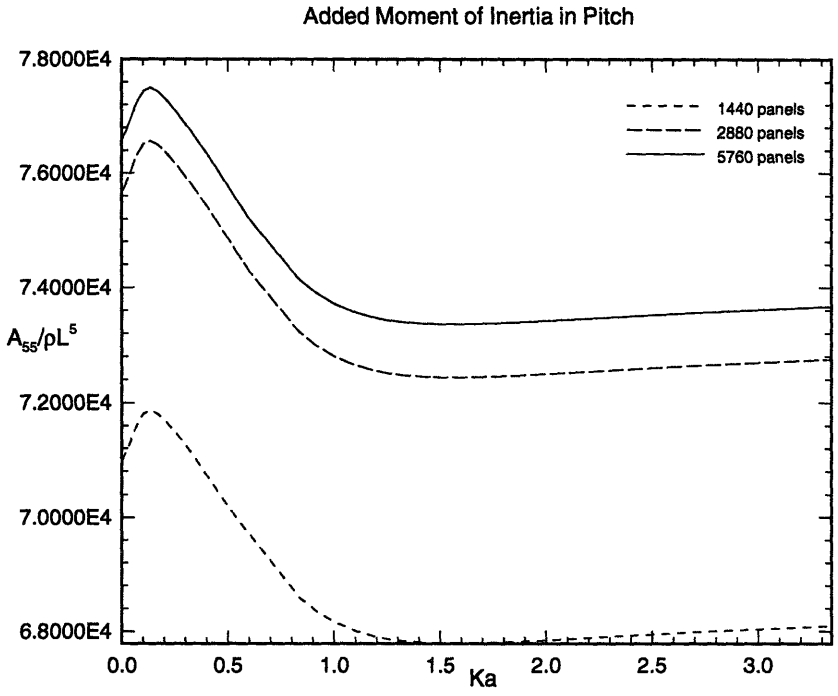

Figure 4-8: Added Moment of Inertia in Pitch for Draugen

converges slowly compared to the surge force and pitch moment with the same number of panels. The reason for this is that the added moment of inertia in pitch is more sensible to the given discretization. The pitch response has its peak at about Ka=1.5, this corresponds to a natural frecuency of 1.3228 rad/sec, which corresponds well with information from the DMI model test. Values of Ka larger than 0.5 do not apply to ocean waves. In the region below Ka=0.5, the response amplitude operator is almost constant and corresponds to a maximum horizontal displacement of the platform deck of 0.165 m for an incident wave of $A = 10m$.

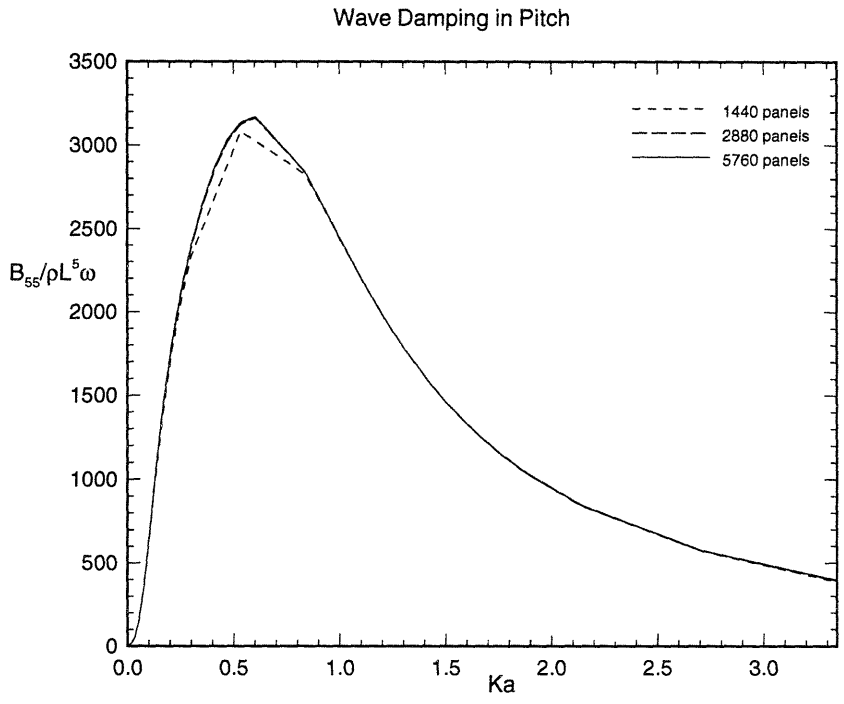

Figure 4-9: Wave Damping in Pitch for Draugen

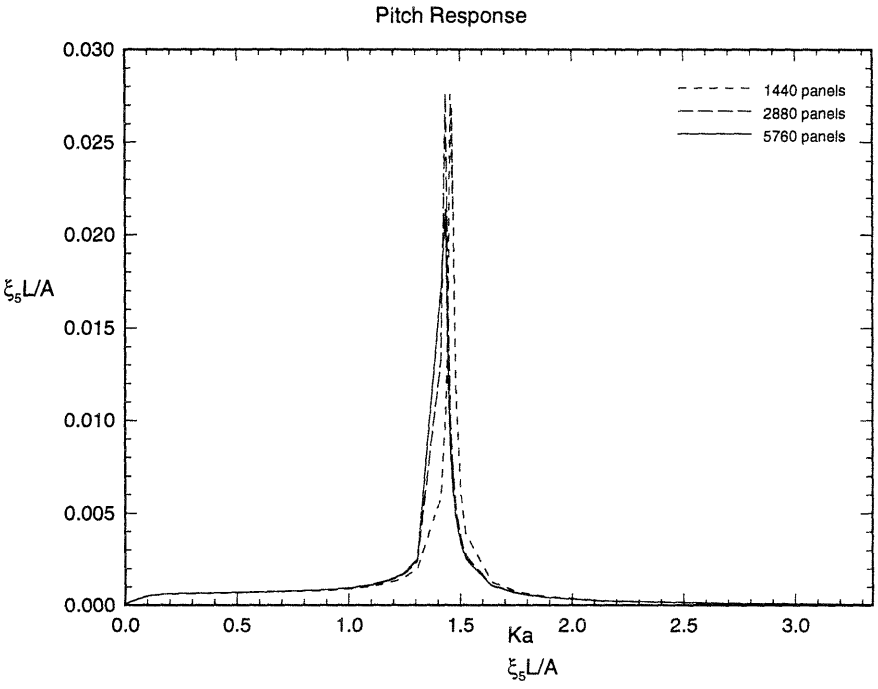

Figure 4-10: Pitch Response of Draugen

4.2 First-Order Solution from the FNV-Theory

The surge force, pitch moment, and pitch response of the cylinder predicted by the FNV-theory is shown and compared with results from WAMIT in figures 4.11-4.16. The results comare well for small values of the nondimensional wavenumber Ka, which corresponds well with the criteria that the FNV-theory is valid in the regime $Ka \ll 1$. It can be concluded from the figures that the FNV-theory is valid for Ka's up to 0.5. For higher frequencies the FNV-theory fails due to the fact that the long wave length approximation is no longer valid.

The pitch response was found from the equation of motion with added moment of inertia and wave damping obtained from WAMIT. In that sense it is not a surprise that the pitch response compares well for lower Ka numbers, since the moment compares well in this region as well.

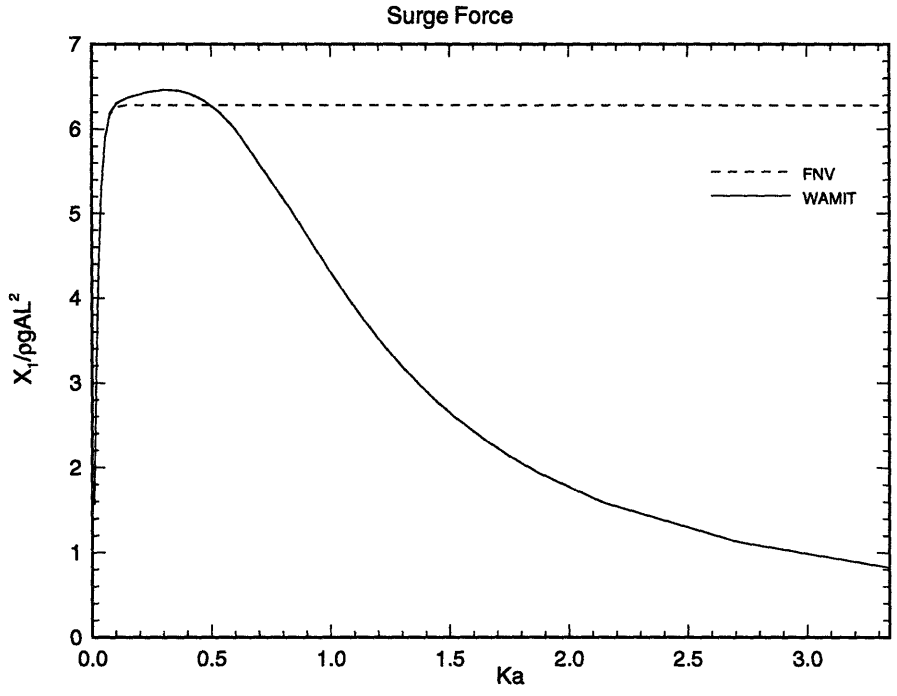

Figure 4-11: First-Order Surge Force Acting on the Cylinder

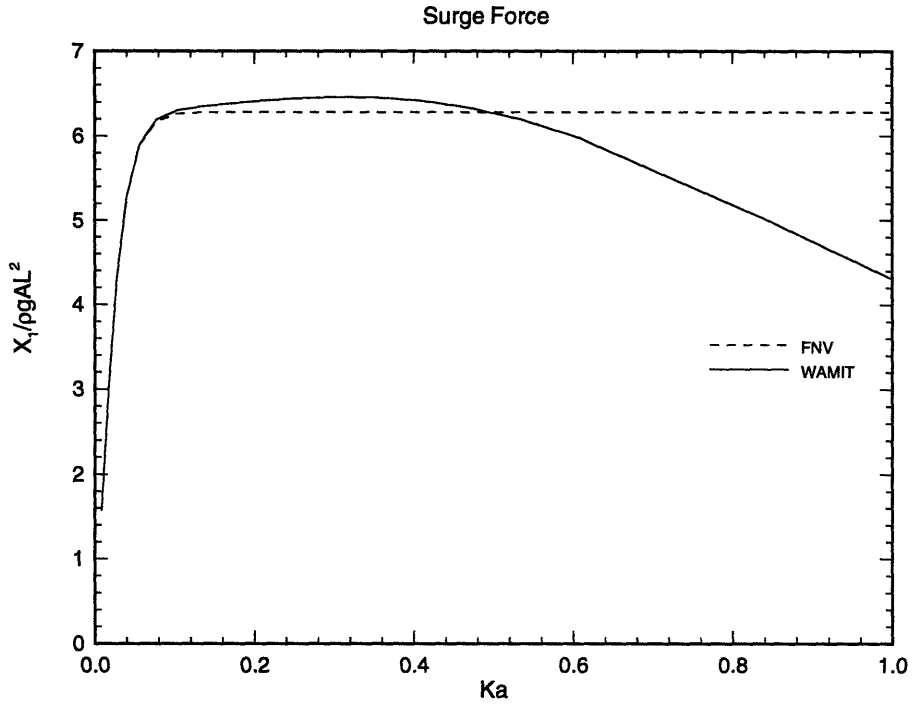

Figure 4-12: First-Order Surge Force Acting on the Cylinder, Close-Up

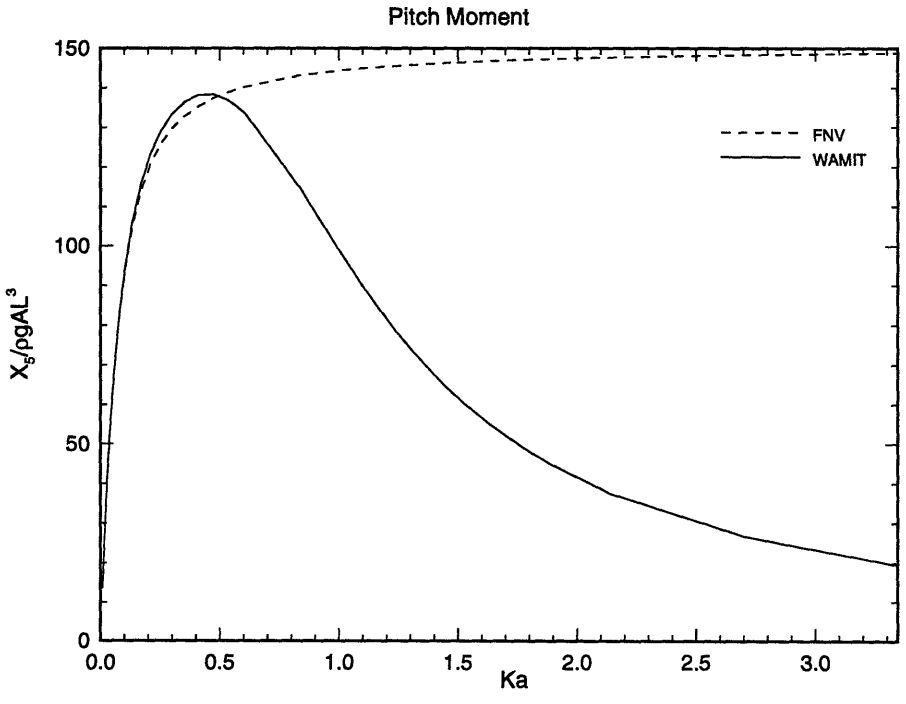

Figure 4-13: First-Order Pitch Moment Acting on the Cylinder

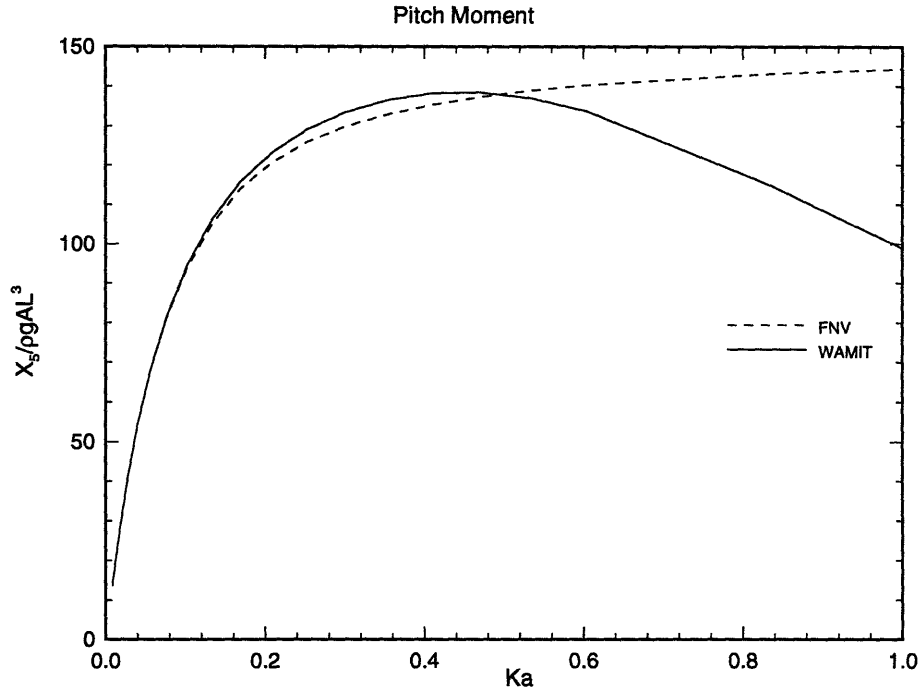

Figure 4-14: First-Order Pitch Moment Acting on the Cylinder, Close-Up

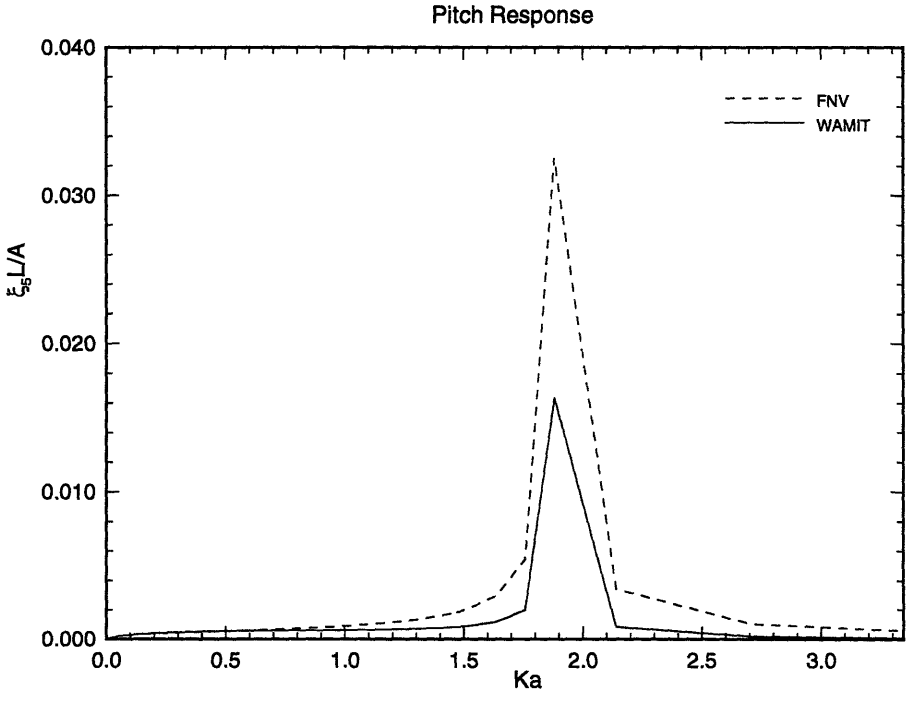

Figure 4-15: First-Order Pitch Response of the Cylinder

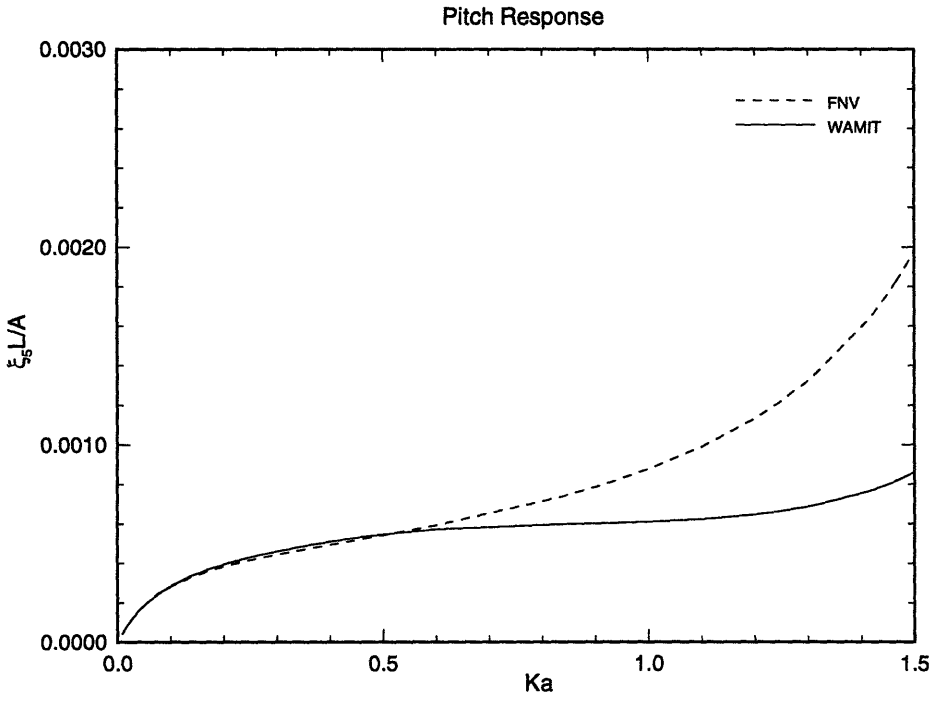

Figure 4-16: First-Order Pitch Response of the Cylinder, Close-Up

Chapter 5

The Higer-Order Solution

For regular incident waves the higer-order force components can be expressed as harmonic time functions as described in Section 2.2.1.. The total force and moment will be a function of first, second, and third harmonics, the moment will also include a fourth harmonic due to the moment arm $(h_1 + \eta_1)$, where h_1 is the distance from the moment point to the mean free-surface, $z = 0$. The higher-order contributions to the surge force and the pitch moment are due to the integrated 2nd-order force plus the "point" forces acting at the free-surface. The total "point" force includes both 2nd and 3rd-order components. Figure 5.1 shows the total "point" force, acting on the free surface, for different Ka values. The time axis is non-dimensionalized such that the fundamental period equals 2 for any Ka value. Two interesting behaviors can be seen in the figure. First, the total "point" force increases in proportion to Ka. Or in other words, the importance of the higher-order "point" forces increases as the waves become steeper. Second, the 2nd and 3rd-order "point" forces tend to reinforce in the first half of the fundamental period, and to cancel during the second half. The moment associated with the "point" forces is shown in figure 5.2. It has the same characteristic as the total "point" force, but it includes a fourth harmonic due to the varying moment arm $(h_1 + \eta_1)$, where $\eta_1 = A \sin \omega t$.

The increasing importance of the higher-order forces with increasing Ka values can be seen in figure 5.3 and 5.4. For $Ka = 0.10$, there is only a slightly difference between the first-order force and the total force acting on the cylinder. For $Ka = 0.30$

the effects of the higher-order forces can be seen to increase and shift the peak value. Figure 5.7 and 5.8 show the increasing higher-order contribution to the total force and moment acting on the cylinder.

In order to compare the significance of the higher-order forces acting on Draugen, the first-order force and moment is obtained from WAMIT. Figures 5.9-5.14 show the higher-order effects on the total force and moment acting on Draugen. One interesting observation is shown in figure 5.13, where the total force actually decreases as Ka increases. The explanation for this can be found by looking at figure 4.6, where the first-order force on Draugen is shown to have a sharp peak at $Ka \approx 0.10$. The higher-order forces are small compared to this peak value.

The excitation moment is periodic with period $\tau = \frac{2\pi}{\omega}$. Thus it can be expanded in a Fourier series as

$$M(t) = \frac{a_0}{2} + \sum_{j=1}^{\infty} a_j \cos j\omega t + \sum_{j=1}^{\infty} b_j \sin j\omega t. \tag{5.1}$$

The only coefficients considered here are a_1, b_2, b_3, and a_4. The steady state pitch motion can be found by solving the linear equation of motion with the forcing function $M(t)$. Using the principle of superposition, the steady state response can be expressed as

$$\begin{aligned}\xi_5(t) = &\sum_{j=1,3} \frac{\frac{a_j}{K_t}}{\sqrt{(1-j^2r^2)^2 + (2\zeta jr)^2}} \cos(j\omega t - \alpha_j) \\ &+ \sum_{j=2,4} \frac{\frac{b_j}{K_t}}{\sqrt{(1-j^2r^2)^2 + (2\zeta jr)^2}} \sin(j\omega t - \alpha_j),\end{aligned} \tag{5.2}$$

where $r = \frac{\omega}{\omega_n}$, ζ is the damping ratio given as

$$\zeta = \frac{B_{55}}{2(I_{EX} + A_{55})\omega_n}, \tag{5.3}$$

and the phase angle α_j is given as

$$\alpha_j = \tan^{-1}(\frac{2\zeta jr}{1 - j^2r^2}). \tag{5.4}$$

From equation (4.11) it can be seen that if $j\omega = \omega_n$ the amplitude of the corresponding harmonic will be comparatively large, and will cause a large response motion. For small values of j and ζ this effect is important. However, for higher values of j the corresponding amplitude becomes smaller and the contribution to the response motion will tend to zero.

The steady state pitch motion in unidirectional regular waves is predicted for Draugen. The added moment of inertia in pitch and wave damping is obtained from WAMIT and used in equation (4.11). Figures 5.15 and 5.16 compares the total response to the first-order response obtained from WAMIT. The results shown are for an incident wave of amplitude $A = 10m$. Figures 5.17 and 5.18 show the overturning moment at the pivot point and the in-deck motion for Draugen. The wave elevation corresponding to figures 5.17 and 5.18 has a mean value of $8.9m$, which is less than the one used in the calculation for the predicted response and moment. However, the peak value (at 240 sec.)in the sample space corresponds to a wave elevation of $10m$ and the in-deck response value compares better with the predicted results as shown in figures 5.15 and 5.16.

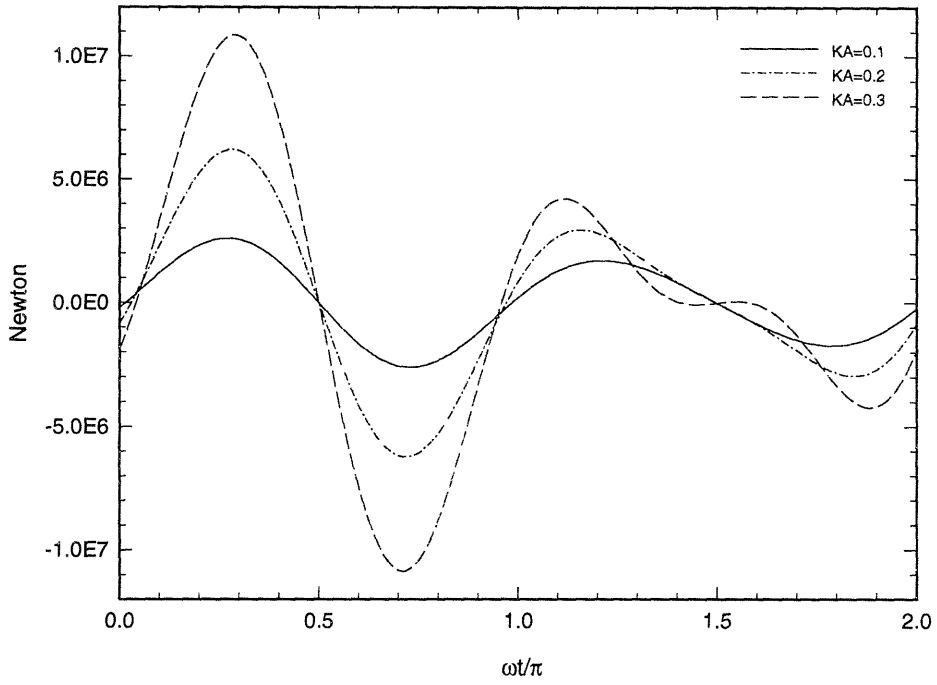

Figure 5-1: Total "Point" Force

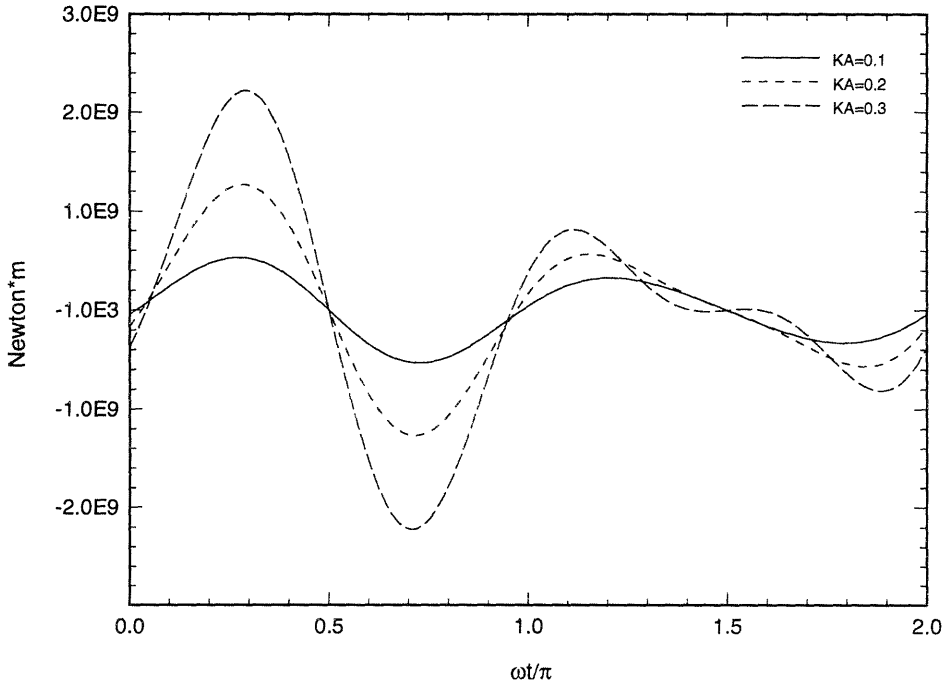

Figure 5-2: Moment due to "Point" Forces

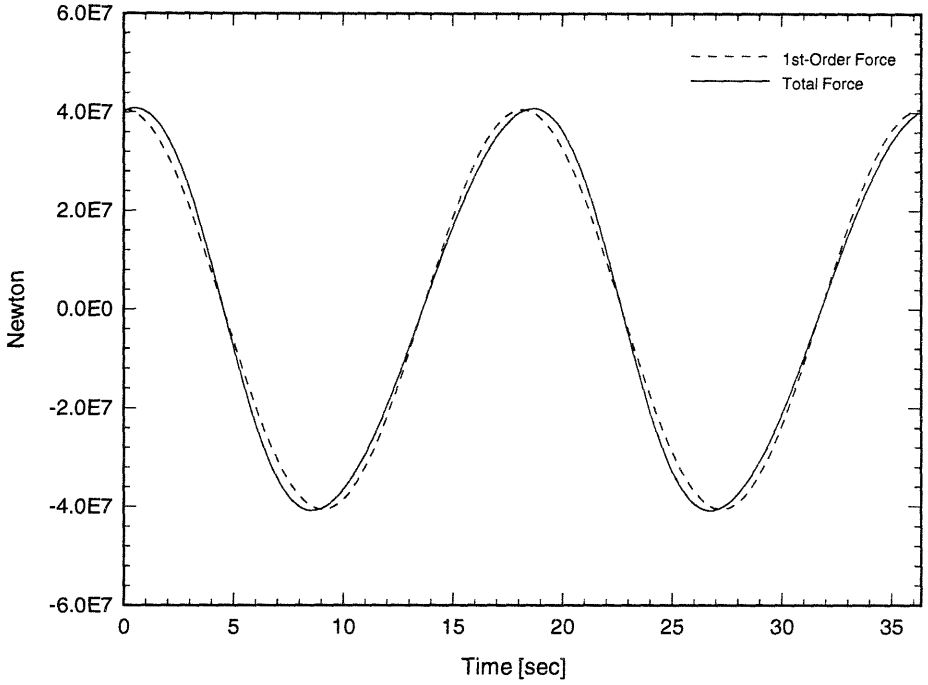

Figure 5-3: Total Force and 1st-order Force on the Cylinder,$Ka = 0.10$

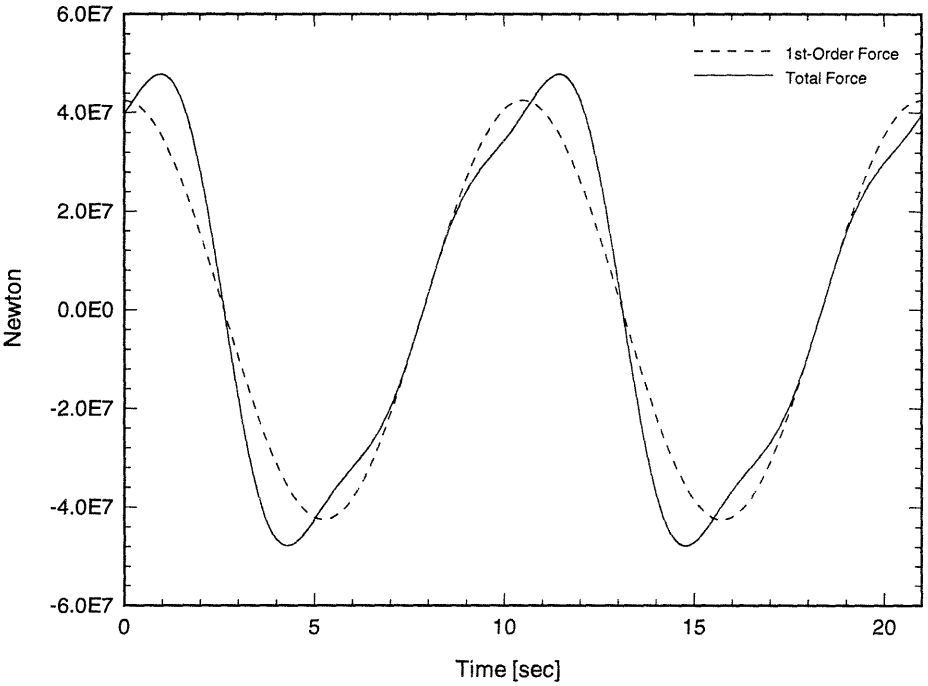

Figure 5-4: Total Force and 1st-Order Force on the Cylinder, $Ka = 0.30$

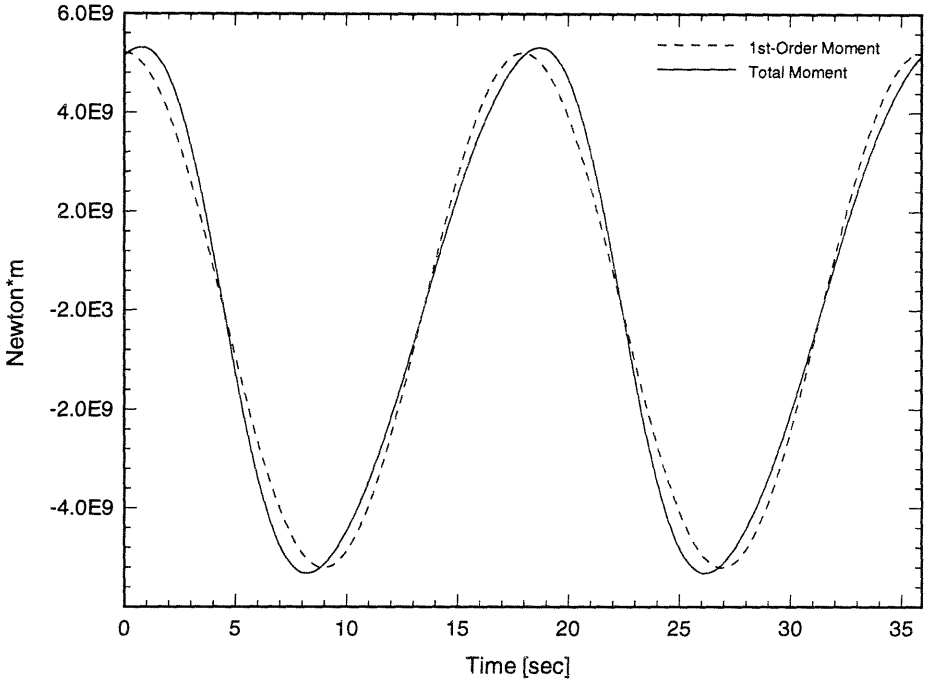

Figure 5-5: Total Moment and 1st-Order Moment on the Cylinder, $Ka = 0.10$

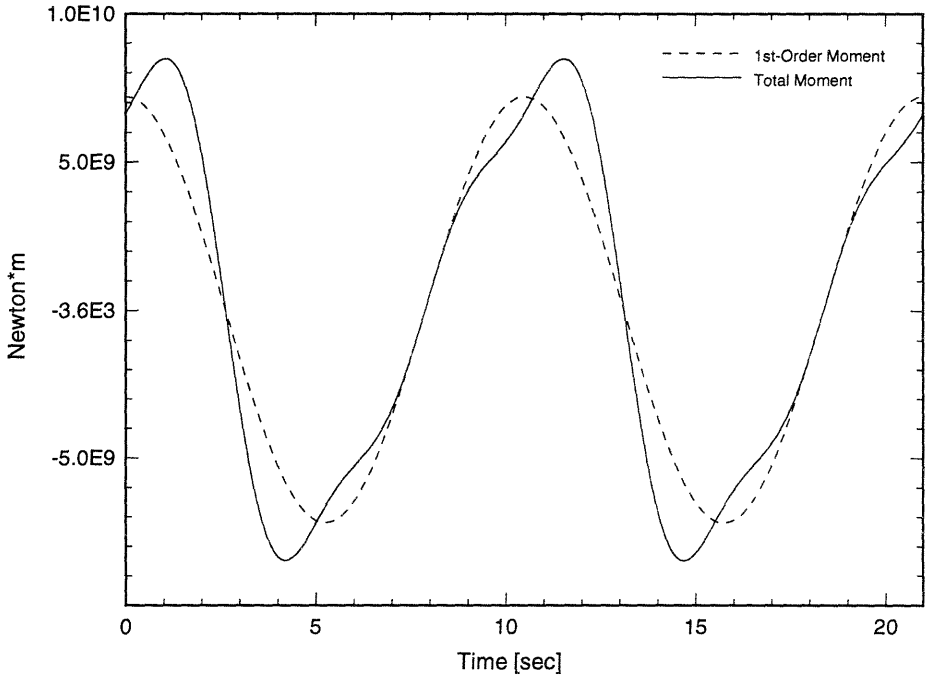

Figure 5-6: Total Moment and 1st-Order Moment on the Cylinder, $Ka = 0.30$

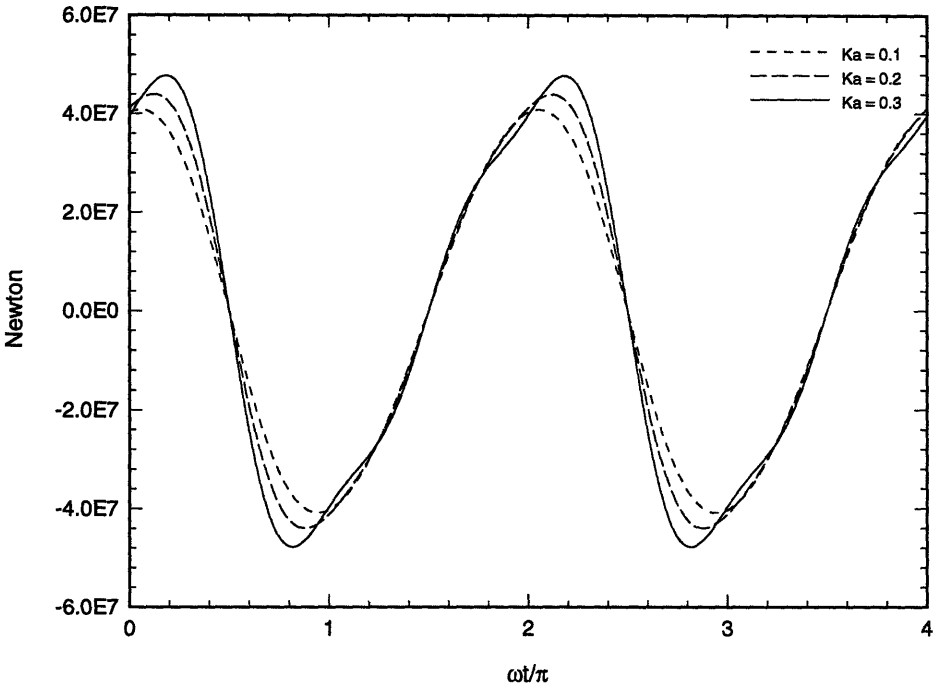

Figure 5-7: Total Force on the Cylinder for Different Ka numbers

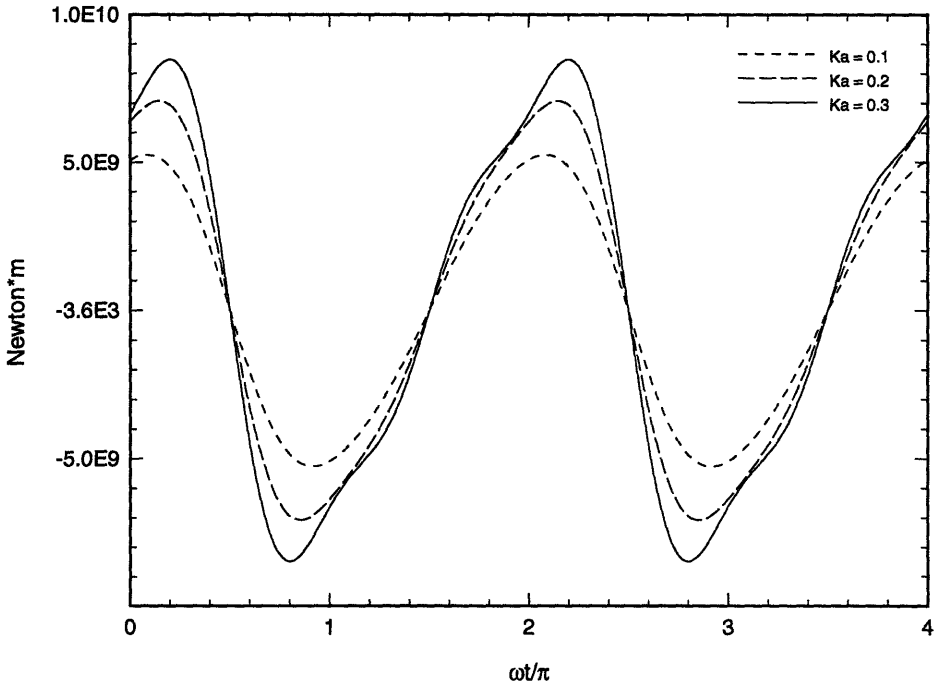

Figure 5-8: Total Moment on the Cylinder for Different Ka numbers

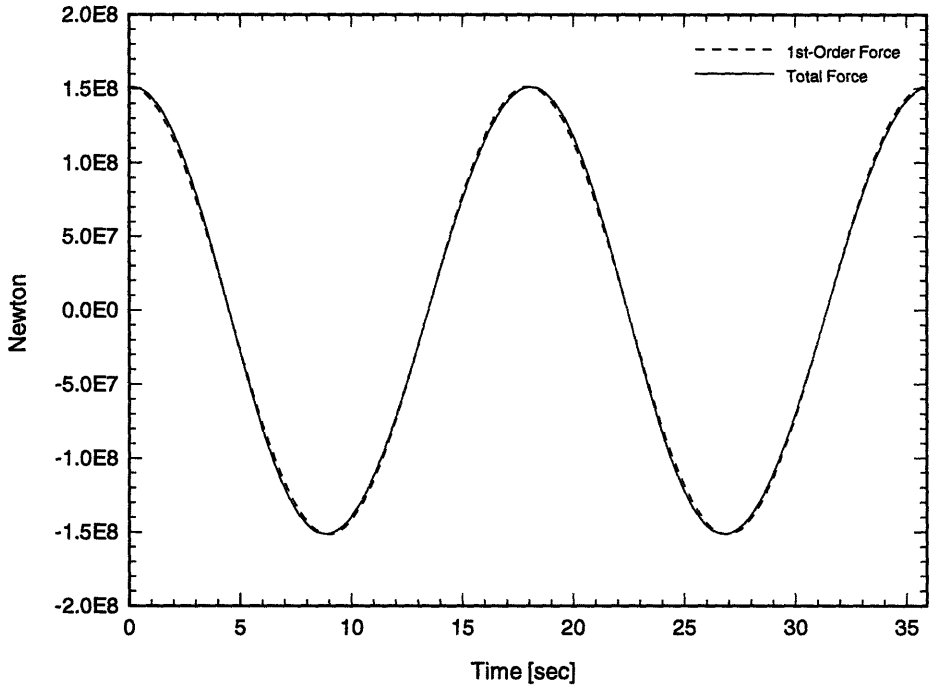

Figure 5-9: Total Force and 1st-Order Force on Draugen, $Ka = 0.10$

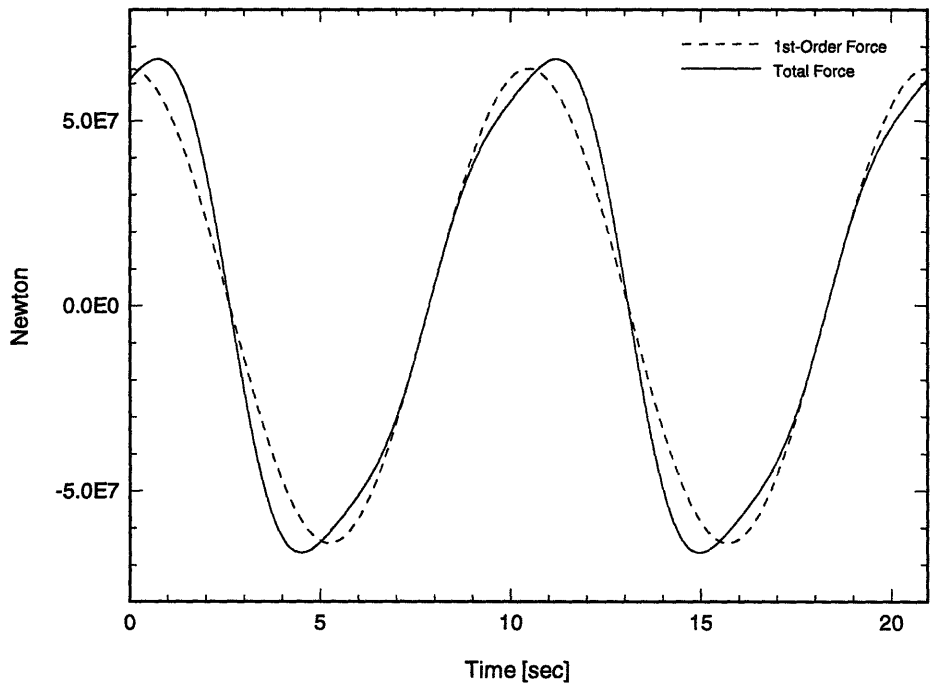

Figure 5-10: Total Force and 1st-Order Force on Draugen, $Ka = 0.30$

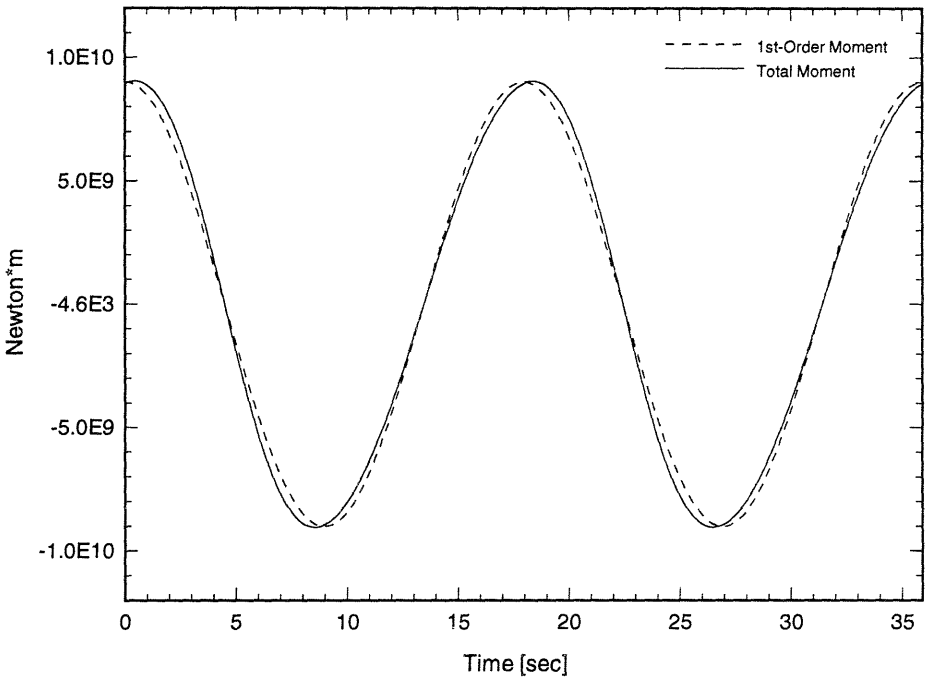

Figure 5-11: Total Moment and 1st-Order Moment on Draugen, $Ka = 0.10$

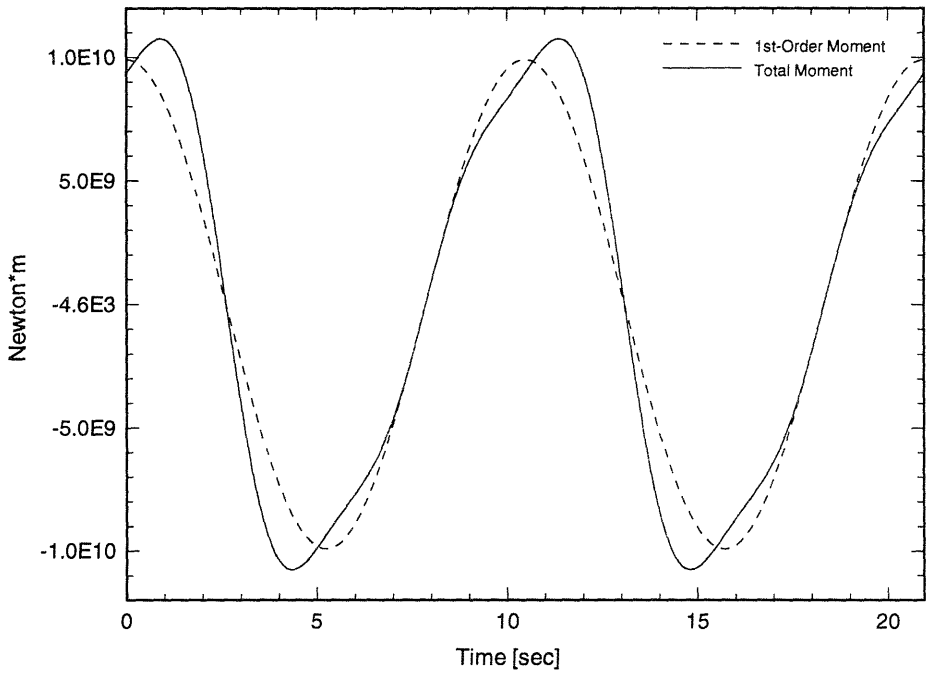

Figure 5-12: Total Moment and 1st-Order Moment on Draugen, $Ka = 0.30$

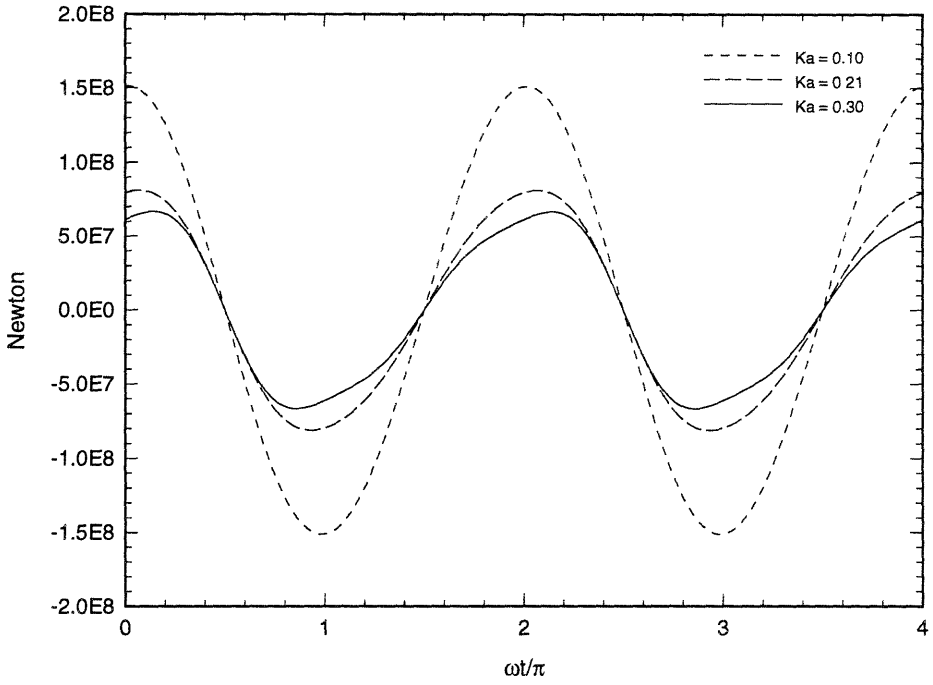

Figure 5-13: Total Force on Draugen for different Ka numbers

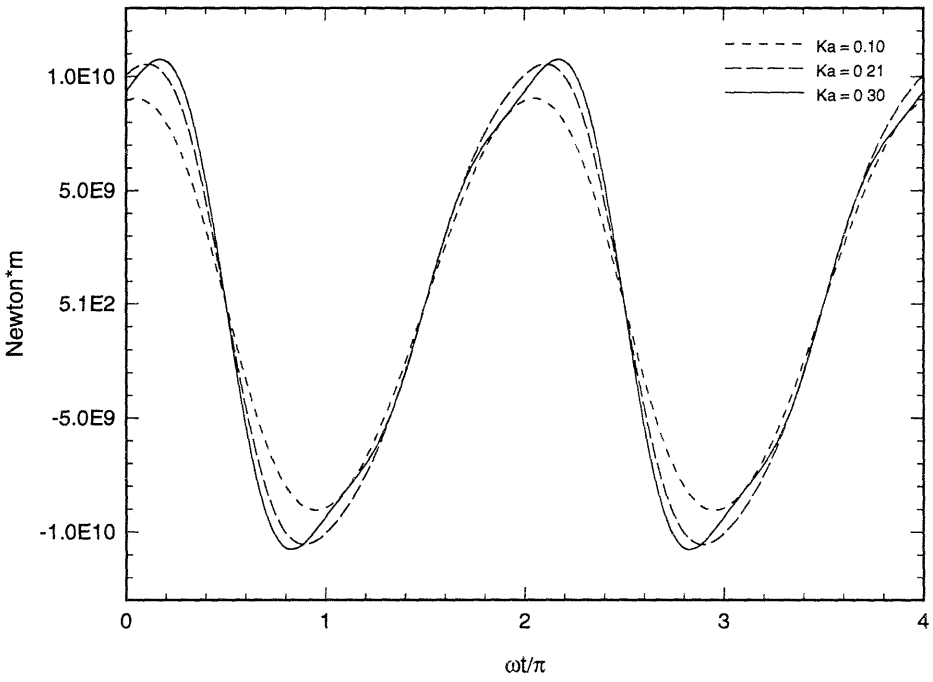

Figure 5-14: Total Moment on Draugen for Different Ka numbers

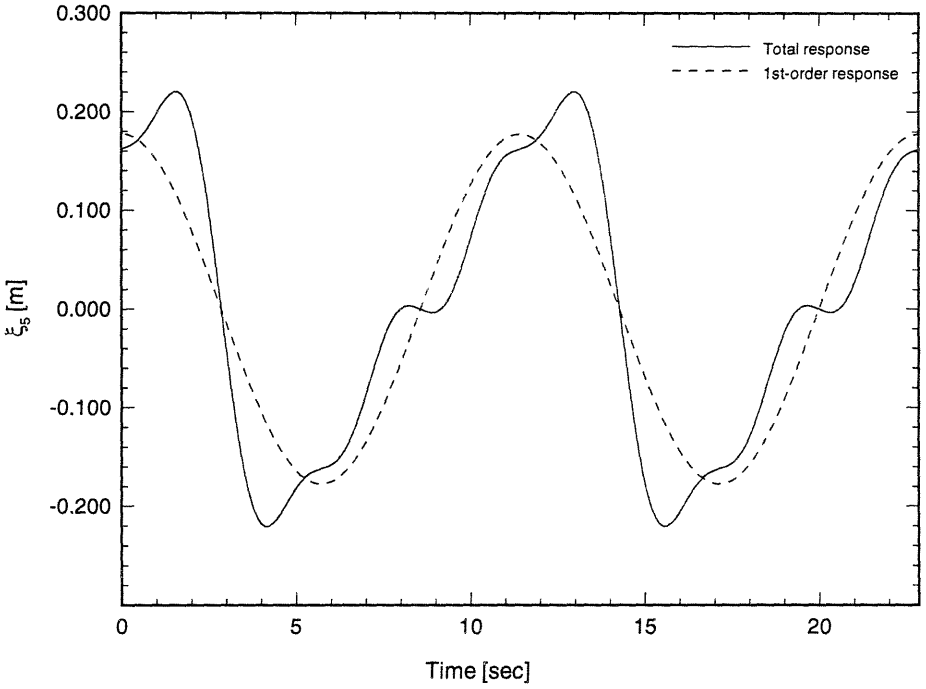

Figure 5-15: Pitch Motion of Draugen, $Ka = 0.25$

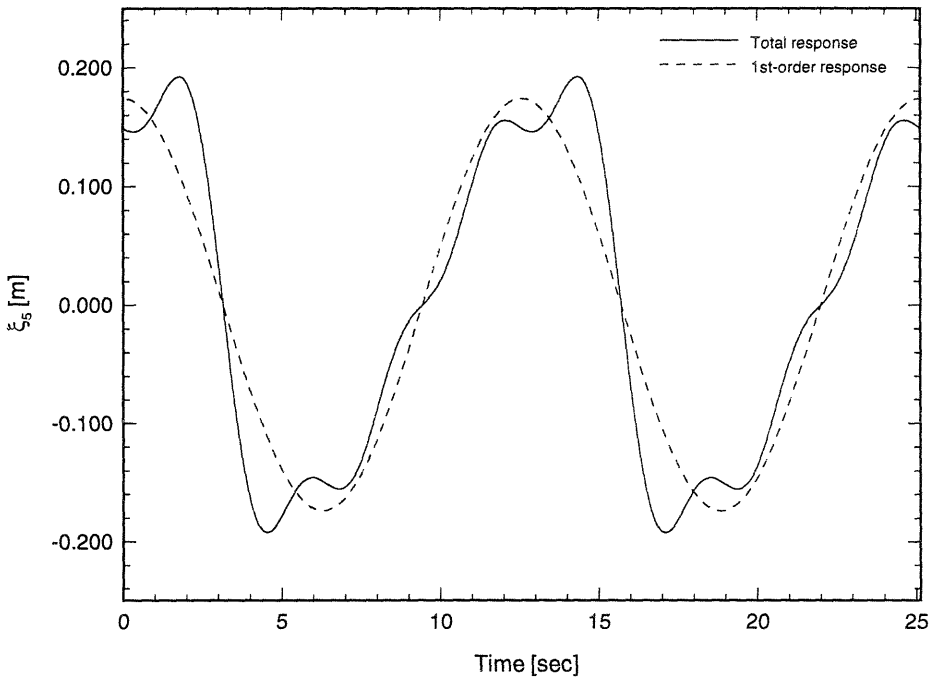

Figure 5-16: Pitch Motion of Draugen, $Ka = 0.21$

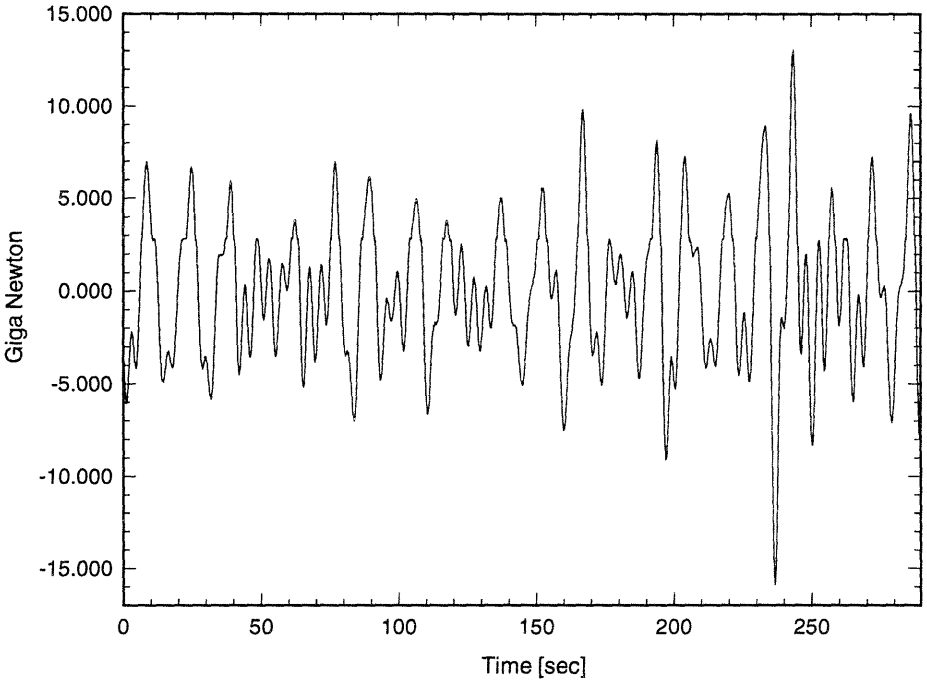

Figure 5-17: Overturning Moment from the DMI-Model Test

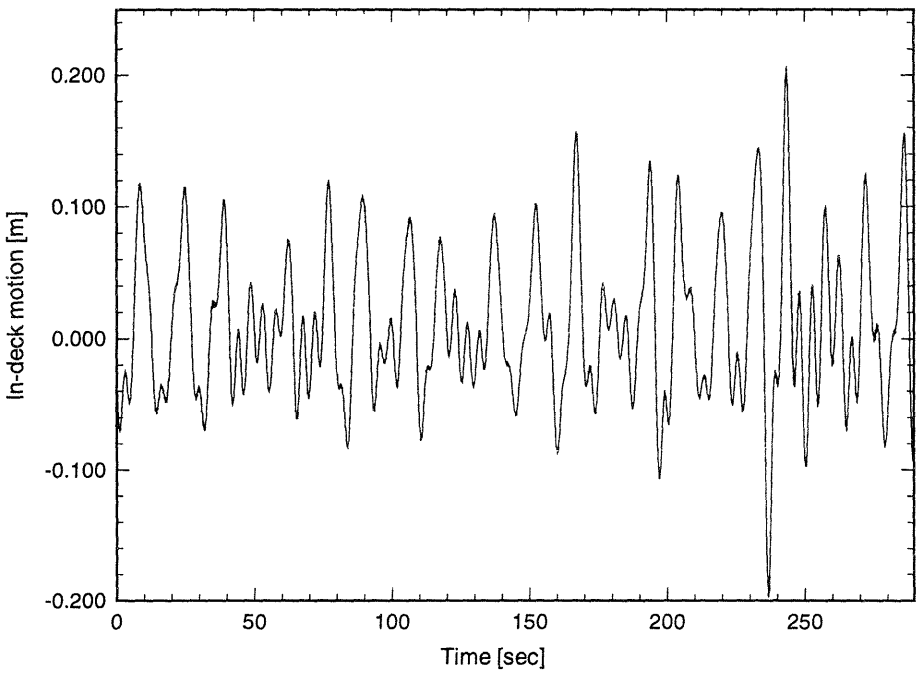

Figure 5-18: In-deck Motion from the DMI-Model Test

Chapter 6

Conclusion

The wave loads up to the third-order are predicted for a cylinder and for the Draugen monotower platform exposed to long waves, based on the FNV-theory. In an inner domain close to the body surface, the wave elevation is assumed to be significantly affected by nonlinearities due to the presence of the structure, causing wave diffraction and scattering. The amplitude A is assumed to be of the same order as the radius a. The higher-order wave forces are concentrated in a region close to the free-surface, and can be thought of as "point" forces acting at the free-surface.

The first-order surge force, pitch moment, and pitch motion for a cylinder and Draugen are obtained from WAMIT and the FNV-results are found to compare well with the WAMIT results for Ka values less than 0.5. The total wave load on Draugen is found by taking the first-order wave load from WAMIT and adding the integrated 2nd-order force and the "point" forces.

The principle of superposition is used to find the steady state pitch response of Draugen from the linear equation of motion. The added moment of inertia and wave damping are obtained from WAMIT. The predicted pitch moment and pitch response are compared to model test results of Draugen and compare well with these results. However, a complete comparison is difficult since only regular waves are considered in this study. A natural next step will be to consider irregular waves.

Bibliography

[1] Dalrymple R. A. and Dean R. G. *Water Wave Mechanics for Engineers and Scientists.* World Scientific, 1991.

[2] McCamy R. C. and R. A. Fuch. Wave forces on a pile: a diffraction theory. Technical Report 69, U.S. Army Board, U.S. Army Corp. of Eng., 1954.

[3] Mei C. C. *The Applied Dynamics of Ocean Surface Waves.* World Scientific, 1989.

[4] Faltinsen O. M., Newman J. N., and T. Vinje. Nonlinear wave loads on a slender vertical cylinder. *Journal of Fluid Mechanics*, 289:179–198, 1995.

[5] Newman J. N. *Marine Hydrodynamics.* MIT Press, 1977.

[6] Newman J. N. Nonlinear scattering of long waves by a vertical cylinder. In *Symposium on Wave and Nonlinear Processes in Hydrodynamics*, Oslo, 1994.

[7] Newman J. N. Wave effects on deformable bodies. *Applied Ocean Research*, 16:47–59, 1994.

[8] Newman J. N. To second order and beyond. In *The Texas section of the Society of Naval Architects and Marine Engineers TLP Technology Symposium*, Houston, 1995.

[9] Jefferys E. R. and Rainey R. T. C. Slender body models of TLP and GBS ringing. In *Proc. 7th International Conference on the Behavior of Offshore Structures*, Cambridge, USA, 1994.

[10] Madsen O. S. Hydrodynamic force on circular cylinders. *Applied Ocean Research*, 8, 1986.

[11] Rao S. S. *Mechanical Viberations.* Addison-Wesley, 1995.

[12] Rainey R. C. T. A new equation for wave loads on offshore structures. *Journal of Fluid Mechanics*, 204:295–324, 1989.

[13] Malenica Š and B. Molin. Third order wave diffraction by a vertical cylinder. *Paper submitted for publication*, 1995.

[14] WAMIT-Manual. *WAMIT: A Radiation-Diffraction Panel Program for Wave-Body Interactions*, version 5.1 edition, 1994.